

**THE REPUBLIC OF TURKEY
BAHCESEHIR UNIVERSITY**

**OPTICAL DETECTION OF SINGLE-
CELL SECRETED ANALYTES ON
SURFACE**

Master's Thesis

MUHAMMAD ATIF PEERWANI

İSTANBUL, 2016

**THE REPUBLIC OF TURKEY
BAHCESEHIR UNIVERSITY**

**GRADUATE SCHOOL OF NATURAL AND APPLIED SCIENCES
BIOENGINEERING**

**OPTICAL DETECTION OF SINGLE-
CELL SECRETED ANALYTES ON
SURFACE**

Master's Thesis

MUHAMMAD ATIF PEERWANI

Supervisor: Assist. Prof. AYCA YALCIN OZKUMUR

İSTANBUL, 2016

**THE REPUBLIC OF TURKEY
BAHCESEHIR UNIVERSITY**

**GRADUATE SCHOOL OF NATURAL AND APPLIED SCIENCES
BIOENGINEERING**

Name of the thesis: Optical detection of single-cell secreted analytes on surface
Name/Last Name of the Student: Muhammad Atif Peerwani
Date of the Defense of Thesis: 12/05/2016

The thesis has been approved by the Graduate School of Natural and Applied Sciences.

Assoc. Prof. Dr. Nafiz ARICA
Graduate School Director

I certify that this thesis meets all the requirements as a thesis for the degree of Master of Sciences.

Assoc. Prof. Dr. Gulay BULUT
Program Coordinator

This is to certify that we have read this thesis and we find it fully adequate in scope, quality and content, as a thesis for the degree of Master of Sciences.

Examining Comittee Members

Signature

Thesis Supervisor
Assist. Prof. Dr. Ayca Yalcin OZKUMUR

Member
Assoc. Prof. Dr. Gulay BULUT

Member
Assist. Prof. Dr. Emre OZKUMUR

ACKNOWLEDGEMENTS

This thesis becomes a reality with the kind support and help of many individuals. I would like to extend my sincere thanks to all of them. First of all, I am thankful to **THE ALMIGHTY ALLAH**, for the wisdom he bestowed upon me, the strength, peace of my mind and good health in order to finish this thesis. I would like to thank my *FAMILY*, for their unceasing encouragement, prayers and support which helped me in completion of this thesis. I would also like to dedicate this work of mine to my *BELOVED MOTHER*. I wish to express my sincere thanks to *BAHCESEHIR UNIVERSITY*, for providing me with all the necessary facilities. I place on record, my sincere gratitude to *TÜBİTAK - Scientific and Technological Research Council of Turkey*, for their financial support through grants 114C122, 113E643 and 115E260. I am extremely grateful and indebted to my thesis supervisor *Assist. Prof., AYCA YALCIN OZKUMUR*, for her expertise, sincere and valuable guidance and encouragement extended to me. I take this opportunity to also thank *Dr. ELIF SEYMOUR, UGUR AYGUN & OGUZHAN AVCI*, for sharing their knowledge and technical know-how whenever I needed. I extend my sincere thanks to *Dr. ONUR SERBEST* of *Sabancı University's Nanotechnology Research and Application Center (SUNUM)*, for training and mentoring me about the nanofabrication part of my thesis. I also place on record, my sense of gratitude to one and all who, directly or indirectly, have lent their helping hand in this work.

12th May, 2016

Muhammad Atif Peerwani

ABSTRACT

OPTICAL DETECTION OF SINGLE-CELL SECRETED ANALYTES ON SURFACE

Muhammad Atif Peerwani

Bioengineering

Thesis Supervisor: Assist. Prof. Ayca Yalcin Ozkumur

May 2016, 50 pages

The human immune system comprises of very complex network of cells. Due to the complexity of human immune system, diagnosis of immune diseases and revealing immunological responses to a pathogen or to interference has been a substantial task. In this paper, we put forward an analytical platform that will re-define our understanding on how intercellular interactions affect the collective response of cell population in an ongoing immune response. This project proposes a system through which monitoring of secretion profile of single-cells in real time becomes possible in quantifiable and radically sensitive way. This competence favors us to identify the previous unknown information about the dynamics of cell secretion and offers access about the effect of kinetic functional behavior carried by an immune response. We started-off constructing prototypes to identify the secretion dynamics of a single cytokine from single-cells, which further helps us to investigate about the collective performance of various types of cells and cytokines that are responsible in the signaling. This non-destructive, digital and real-time monitoring of isolated single-cells secretion will let us uplift technological advancements to a next-level.

Keywords: Digital Detection, Microengraving, Interferometry, Optical Biosensor, Dynamic Monitoring.

ÖZET

TEK HÜCRE DEN SALGILANAN MATERYALLERİN BİR YÜZEY ÜZERİNDEN OPTİK OLARAK ALGILANMASI

Muhammad Atif Peerwani

Biyo Mühendisliği

Tez Danışmanı: Yrd. Doç., Ayca Yalcin Ozkumur

Mayıs 2016, 50 sayfalar

İnsan bağışıklık sistemi kompleks bir hücre ağından oluşmaktadır. Bu kompleks yapı bağışıklık sistemi hastalıklarına tanı konulmasını ve bu ağın bir patojene tepkisinin incelenmesini önemli bir problem haline getirmiştir. Bu çalışmada hücreler arası etkileşimlerin, bir bağışıklık tepkisi anında hücre popülasyonlarının kollektif tepkisini nasıl etkilediğinin gözlemlenebileceği bir platform ortaya geliştirilmiştir. Çalışma içerisinde gerçek zamanlı olarak tek hücrelerin salgı profillerinin hassas bir şekilde ölçülebileceği bir sistem önerilmiştir. Bu sistem hücre salınım dinamikleri hakkında daha önceden bilinmeyen bilgilere erişim imkanı sağlamakla birlikte, bağışıklık tepkisiyle birlikte oluşturulan kinetik fonksiyonel davranışların etkisinin de belirlenmesini sağlamaktadır. Tek bir hücrenin sitokin (cytokine) salgı dinamiklerinin belirlenmesi için prototip geliştirilmiştir. Geliştirilmiş olan dijital, hasarsız ve gerçek zamanlı tek-hücre sitokin salgı izleme sistemi, bu alandaki teknolojik gelişmeleri bir üst düzeye taşıyacaktır.

Anahtar Kelimeler: Dijital Algılama, Mikro-İsleme, Interferometri, Optik Biyoalgılayıcı, Nano-Parçacık, Dinamik Gözlemeleme.

CONTENTS

| | |
|--|-----------|
| FIGURES | ix |
| ABBREVIATIONS | xi |
| 1. INTRODUCTION | 1 |
| 1.1 OVERVIEW | 1 |
| 1.2 TECHNIQUES FOR MEASURING CYTOKINE SECRETIONS | 2 |
| 1.2.1 Enzyme Linked Immunosorbent Assay | 2 |
| 1.2.2 Enzyme Linked Immunosorbent Spot | 3 |
| 1.2.3 Intracellular Staining (ICS) | 4 |
| 1.3 PROPOSED METHODOLOGY | 5 |
| 2. OPTICAL DETECTION | 9 |
| 2.1 DETECTION APPROACH | 9 |
| 2.2 INSTRUMENT | 10 |
| 2.3 LABELING NANOPARTICLES FOR SINGLE PARTICLE DETECTION | 12 |
| 2.4 CONCLUSION | 12 |
| 3. NANOWELL FABRICATION | 13 |
| 3.1 INTRODUCTION | 13 |
| 3.2 MASK DESIGNS | 13 |
| 3.3 FABRICATION PROTOCOL | 16 |
| 3.4 POST-FABRICATION RESULTS | 17 |
| 3.5 DISCUSSION AND CONCLUSION | 24 |
| 4. NUMERICAL SIMULATIONS OF THE NANOWELL SYSTEM | 25 |
| 4.1 DEFINING THE MODEL | 25 |
| 4.1.1 Physical Model | 25 |

| | |
|--|----|
| 4.1.2 Assumptions for Simplification of the Model | 26 |
| 4.2 MATHEMATICAL EQUATIONS | 26 |
| 4.3 RESULTS..... | 28 |
| 4.4 EFFECTS OF MODEL PARAMETERS ON SIMULATION RESULTS.... | 30 |
| 4.4.1 Effect of the Equilibrium Dissociation Constant (K_D)..... | 30 |
| 4.4.2 Effect of Rate of Secretion (k) | 31 |
| 4.4.3 Effect of Nanowell Size | 33 |
| 4.4.4 Effect of the Position of the Reaction Surface | 34 |
| 4.5 DISCUSSION | 35 |
| 5. CONCLUSION..... | 37 |
| REFERENCES..... | 38 |

FIGURES

| | |
|--|----|
| Figure 1.1: Stepwise procedure of ELISA | 2 |
| Figure 1.2: Detection of cytokines via ELISpot..... | 4 |
| Figure 1.3: Illustrates stepwise working of ICS..... | 5 |
| Figure 1.4: Illustration of serial microengraving to monitor cytokine secretion by single cells in time. | 6 |
| Figure 1.5: The key to improved visibility of nanoparticles on the SP-IRIS system is the mixing of scattered light with reference light reflected from the Si-SiO ₂ interface. | 7 |
| Figure 2.1: Optical arrangement of single particle IRIS system..... | 9 |
| Figure 2.2: The SP-IRIS instrument | 10 |
| Figure 2.3: The GUI of the acquisition software | 11 |
| Figure 2.4: Detection via nano-barcode feature..... | 12 |
| Figure 3.1: Mask design to create 50x50 micron wells. | 14 |
| Figure 3.2: Mask design to create 70x70 micron wells. | 14 |
| Figure 3.3: Mask design to create 100x100 micron wells. | 15 |
| Figure 3.4: Mask design to create 150x150 micron wells. | 15 |
| Figure 3.5: Steps of fabrication..... | 17 |
| Figure 3.6: Post-fabricated mask with labeled dimensions of all four mask designs. | 18 |
| Figure 3.7: Post-fabrication-microscope images (50X) displaying dimensions of well-sizes..... | 19 |
| Figure 3.8: Post fabrication profiler results measuring resist thickness of (150x150) wells to be 58 microns. | 20 |
| Figure 3.9: Profiler measurements for well-depth of the 100 micron nanowell array | 20 |
| Figure 3.10: Profiler measurements for the 50 micron wells. A non-uniform well depth is observed..... | 21 |
| Figure 3.11: Profiler measurements for the 50 micron wells after increasing developing time. The non-uniformity in well depth is still visible..... | 21 |
| Figure 3.12: Profiler measurements for 4,6 and 8 seconds of exposure time. a) 50x50 micron wells, b) 70x70 micron wells, c)100x100 micron wells..... | 22 |
| Figure 4.1: Schematics of a nanowell containing a single cell | 25 |

| | |
|--|----|
| Figure 4.2: Heat map to visualize concentration distribution in volume using same physical parameters as shown in Table 4.1. Total incubation time is 30 hours..... | 29 |
| Figure 4.3: Plots of the calculated quantity of analytes accumulated in nanowell and on the bottom surface during microengraving when the cell secretes at a constant rate of 10 molecules/s. | 30 |
| Figure 4.4: Graph showing decrease in surface concentration with the increase in K_D . | 31 |
| Figure 4.5: Graph shows surface concentration saturation trend with the increase in secretion rate | 32 |
| Figure 4.6: Graph illustrates trend of increase in number of analytes in cubic volume with the increase in secretion rate (k) | 33 |
| Figure 4.7: Plot showing the number of analytes accumulated in the nanowell and on the bottom surface during microengraving using same parameters as in Table 4.1 except (a) well size of (50x50x50) μm with cell being incubated for 30 hours (b) well size of (70x70x50) μm (c) (100x100x50) μm , with cell being incubated for 40 hours..... | 34 |
| Figure 4.8: Graph showing the number of analytes in nanowell and on the glass surface positioned on top when the cell secretes 10 molecules/s with a dissociation constant $K_D=100\text{pM}$ and density of binding sites of 10^{-9}mol/m^2 | 35 |

ABBREVIATIONS

| | | |
|---------|---|---|
| CAD | : | Computer-aided drafting |
| CCD | : | <i>Charge-Coupled Device</i> |
| ELISA | : | Enzyme Linked Immunosorbent Assay |
| ELISPOT | : | Enzyme Linked Immunosorbent Spot |
| ES | : | Elevation Stage |
| GUI | : | Graphical User Interface |
| ICS | : | IntraCellular Staining |
| IPA | : | IsoPropyl Alcohol |
| IRIS | : | Interferometric Reflectance Imaging Sensor |
| K | : | Effect of rate of secretion |
| K_D | : | Equilibrium Dissociation Constant |
| LED | : | Light Emitting Dide |
| NA | : | Numerical Aperature |
| PDMS | : | PolyDiMethylSiloxane |
| PVDC | : | PolyVinylidene Chloride |
| RPM | : | Revolutions Per Minute |
| SP-IRIS | : | Single-Particle Interferometric Reflectance Imaging Sensor |
| SUNUM | : | Sabancı University's Nanotechnology Research and Application Center |
| USA | : | United States of America |
| UV | : | UltraViolet |

1. INTRODUCTION

1.1 OVERVIEW

Cellular functions, lineages, and clonotypic breadth varies widely among cells in a clinical sample. Conventional methods cannot describe the role of constituent members and interactions between the intricate meshwork of cells and therefore fail short in analyzing, defining and assessing the complexity of the human immune cells network. Additionally, there are many factors such as the environment or imposed stimuli, which promote changes in the biological sample, ultimately resulting in a different response in relation to an input. A major limiting factor of a conventional measurement analysis is monitoring the behavior of cells at discrete intervals of time. Dynamic functional analysis of cells will provide us potential insights regarding the functional variance among cells over a period of the timescale.

One of the most important ways by which immune responses are regulated is through intercellular communication by cytokines. Cytokines are cell signalling proteins produced by immune cells, fibroblasts, stromal cells and endothelial cells. They help in cell to cell communication mainly during immune responses and stimulate the movement of cells towards site of infection or inflammation. As they circulate in picomolar concentration, they have high magnitude response to an infection or inflammation in comparison to a hormone (1). Understanding the expression and secretion of cytokines is crucial in understanding their role in disease progression and how different cell types respond to various therapies. It is worthwhile to mention that it is essential to analyze the secretion dynamics of the cytokine production. This is so because the cytokine responses may be short term, delayed, sustained or long lasting. Real time monitoring of cytokine secretion would facilitate analysis of the secretion dynamics during an immune response.

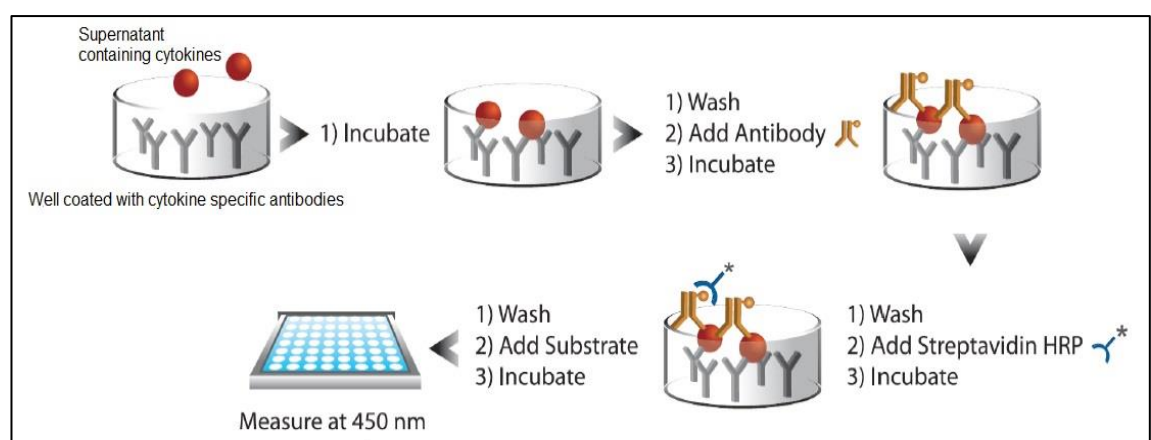
1.2 TECHNIQUES FOR MEASURING CYTOKINE SECRETIONS

Determining the kinetics of cytokine secretion is not trivial. Various methodologies have been developed to date for measuring cytokine secretion including intracellular staining (ICS), enzyme linked immunosorbent spot (ELIspot), biocarbode assay and digital ELISA.

1.2.1 Enzyme Linked Immunosorbent Assay

Enzyme Linked Immunosorbent Assay (ELISA) is a commonly used technique for the determination of known analytes. The ELISA Assay is dependent upon the underlying level of immunoreactivity of the target antibodies of the analyte (2). The typical steps of ELISA includes recognition and binding to the target molecule later followed by the detection of the bound target. In this technique, antibodies are applied to the well of microtiter plate. The capture antibody then binds to the plate via adsorption to the surface. A blocking solution is applied in order to adhere to any available vacant sites. After incubation phase, sample plate is washed and treated with enzyme linked detection antibody. The reaction is terminated with the addition of chromogenic catalysis substances (Figure 1-1).

Figure 1.1: Stepwise procedure of ELISA



Source: Enzo Life Sciences. (2009). Immunoassays – ELISA kits. Product Guide, 5-6. (3)

Recently, ELISA have shown a big transition from transforming to chromogenic substances to fluorogenic substances. Chromogenic substances give the detectable color as change whereas fluorogenic substances emits lights as the signal output. There is increased sensitivity in fluorogenic detection in comparison to the chromogenic detection substrates. ELISA detection is based on direct and indirect detection principles. In indirect detection method, a secondary antibody is used which is responsible for recognition and binding to the specific immunoglobulins. ELISA is a versatile and a sensitive method which offers a reasonable method for the detection of multiple epitopes (4).

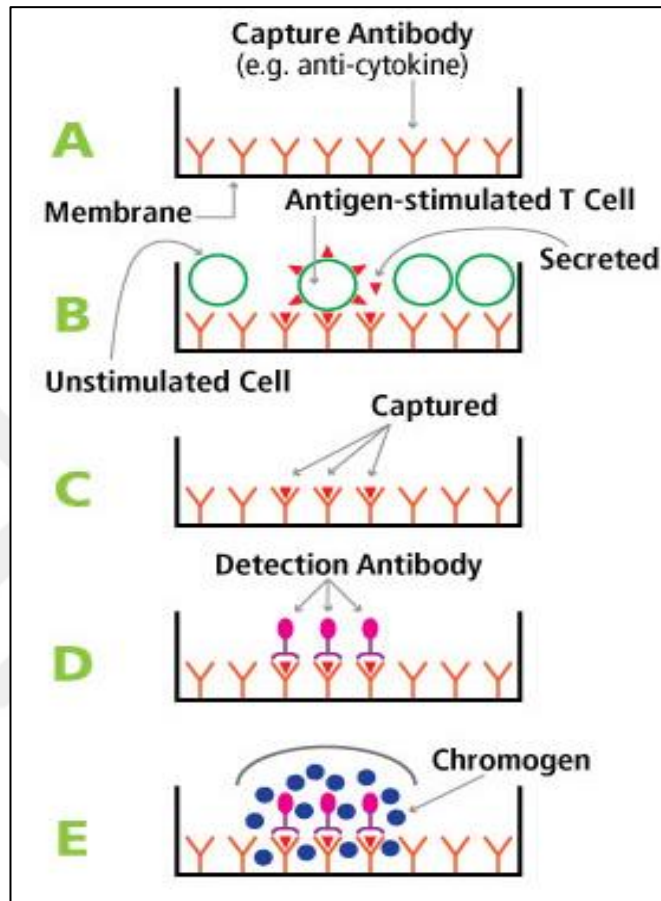
1.2.2 Enzyme Linked Immunosorbent Spot

Enzyme Linked Immunosorbent Spot, commonly known as ELISpot, was originally developed to enumerate B cells secreting antibodies against antigens (5). ELISpot is now adapted for enumeration and identification of cytokine secreting cells at cellular level. The method is identical to Enzyme Linked Immunosorbent Assay (ELISA) with minor variations (6). The ELISpot assay enables the identification, quantification and analysis of the activated and responding cells at a single cell level. The assay allows the quantification of rare cell populations such as antigen antibody specific responses (7).

The ELISpot capture antibody is coated onto a polyvinylidene difluoride (PVDC) backed micro-well plate. The plate is then blocked with serum proteins. Cells of interest are then plated at varying densities and incubated at 37 degrees. Analytes secreted by activated cells are captured locally by the coated antibody on the PVDC membrane. The micro-wells are then washed to remove unbound cells, cellular debris and other media components. A second antibody which is biotinylated binds to the distinct epitope of the target, such as cytokines. Addition of the chromogen after this allows visualization of colored spots around cytokine secreting cells (Figure 1-2). The spots then can be counted manually or using an automated reader in order to capture images which will provide a detailed insight regarding the number and size of spots (6). ELISpot is successfully utilized in detection of interferon—gamma and interleukin 5 producing cells as a predictive market for renal allograft. In addition to that, it is an important post-

transplant reactivity tool which is significantly useful in monitoring immune responses (5).

Figure 1.2: Detection of cytokines via ELISpot



Source: Cellular Technology Limited. (2008). How ELISPOT Assays Work: ImmunoSpot Platform for ELISPOT, Bacterial Colonies, and Viral Plaque. Protocols. (8)

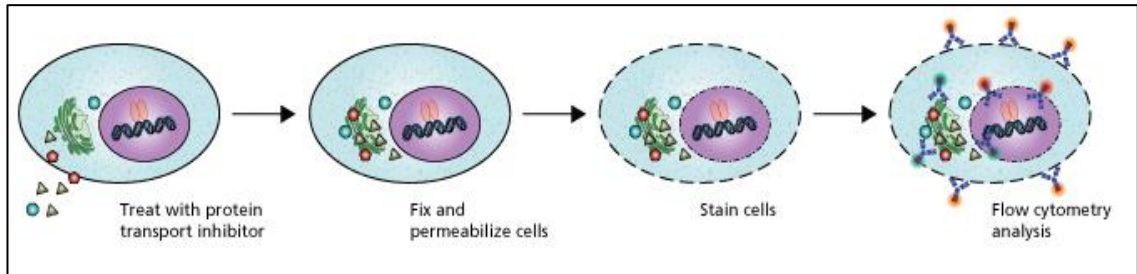
1.2.3 Intracellular Staining (ICS)

Intracellular staining is commonly used for visualizing proteins accumulated within cells. The method involves the following steps (Figure 1-3):

- Cells are first treated with protein transport inhibitor to allow accumulation of target protein inside the cell.
- Cells are fixed and subjected to permeabilization allowing the antibody to enter the nucleus.

- c. Staining the cells intracellularly with fluorescent antibodies.
- d. Cells are then analyzed by flow cytometry.

Figure 1.3: Illustrates stepwise working of ICS



Source: BD Biosciences Research. (2012). Intracellular Flow. Research Application. Techniques. (9)

Intracellular cytokine staining combined with flow cytometry has the specific advantage of enabling simultaneous assessment of multiple phenotypic, differentiation and functional parameters pertaining to immune cells (10). Therefore, these attributes of intracellular cytokine staining makes it suitable for the assessment of immune responses.

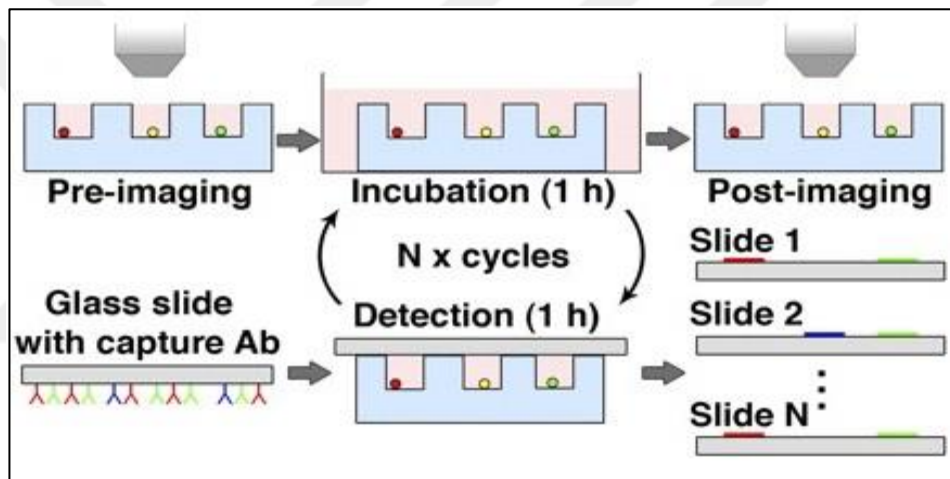
1.3 PROPOSED METHODOLOGY

Intracellular staining coupled with flow cytometry is used to assess the secretion of cytokines in an indirect fashion, as the measured amount of cytokines are not necessarily secreted. Since flow cytometry requires fixation of the cells, the method is also destructive to the viability of the cells. ELISPOT fails to provide quantitative analysis of the cytokines secreted from the cells and the cells are lost during the process. Biocarbode assay and digital ELISA works similarly except that secreted supernatant is collected from specific cell types and poured for incubation on the surface of the prepared microwell. For biocarbode assays the complexes are tagged via metal (gold, silver) nanoparticles for optical detection. They have high sensitivity and specificity, but are unable to offer real time monitoring.

A recent method developed by Love, et al. (11), called ‘microengraving’ allows for quantitative measurement of cytokine secretion (Figure 1-4). In this technique, single

cells are isolated in an array of nanoliter-sized wells, which are enclosed with a glass coverslip forming microenvironments for individual cells. Secreted analytes from these individual cells can be captured on the coverslip. Analysis of the glass slide with captured analytes using secondary antibodies tagged with fluorophores and by detecting the fluorescence signal at any instant reveals the amount of cytokines bound, which correlates to the amount secreted. Repetition of the method with serial end-point measurements gives previously unattainable information about cytokine secretion dynamics (12).

Figure 1.4: Illustration of serial microengraving to monitor cytokine secretion by single cells in time.

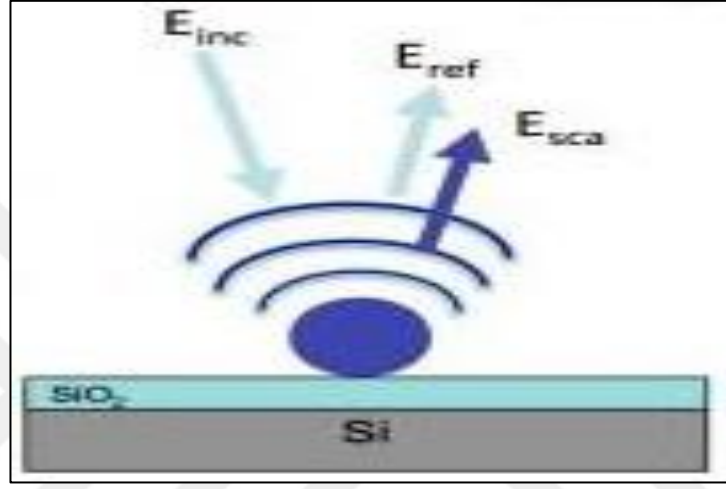


Source: Beiyuan, F., Li, X., Chen, D., Peng, H., Wang, J., and Chen, J. (2016). Development of Microfluidic Systems Enabling High-Throughput Single-Cell Protein Characterization.. *Sensors* 16.2 :232. (13)

However, this method does not provide real-time monitoring. Moreover, switching of slides requires opening and closing of nanowells, which also affects the microenvironment. To overcome these challenges, here we propose a novel method to reveal the functional dynamics of cytokine secretion through real-time monitoring of the secretion profile of the immune cells. Our method combines microengraving with an optical single-particle detection technique, called Single-Particle Interferometric Reflectance Imaging Sensor (SP-IRIS).

The detection principle of SP-IRIS developed by Unlu, et al. (14) is based on enhanced contrast in the scattering signal from nanoparticles on a layered substrate as shown in Figure 1-5 (15).

Figure 1.5: The key to improved visibility of nanoparticles on the SP-IRIS system is the mixing of scattered light with reference light reflected from the Si-SiO₂ interface.



SP-IRIS allows detection and quantification of nanoparticles by interfering the scattering from the nanoparticle with the reflection from a buried layer (Equation 1). The thickness of the top layer (oxide) is responsible for phase changes between the scattered and reflected signals, and results in a change in contrast of the particle of interest.

$$I \propto |E_{ref}|^2 + |E_{sca}|^2 + 2|E_{ref}||E_{sca}| \cos \theta \quad (\text{Eq. 1})$$

$$|E_{sca}|^2 \propto \alpha^2 \quad (\text{Eq. 2})$$

$$\alpha = 4\pi\epsilon_0 r^3 \frac{\epsilon_p - \epsilon_m}{\epsilon_p + 2\epsilon_m} \quad (\text{Eq. 3})$$

Here, the α is the polarizability of the particle, E_{ref} is the electric field of the reference (reflected) light, θ is the phase lag between the reference and scattered fields. For small

particles having radius to the scale of 10^{-9} , $|E_{sca}|^2$ becomes negligible in the above equation which means term $2|E_{ref}||E_{sca}|\cos\theta$ dominates the signal from the nanoparticles. The size of the particle can therefore be calculated from the contrast of the detected particle (15).

Using SP-IRIS, metallic particles with diameters greater than 20nm and dielectric particles with diameters greater than 60nm have been successfully detected (16). The method has been applied to detection of proteins, DNA and whole pathogens (virions) (17).

In this work, we aim to develop a new method to enable answering questions regarding the nature of cytokine secretion. Our specific goals within the scope of this thesis are:

- a. Create the tools that will enable real-time monitoring of cytokine secretion.
 - i. Fabricate nanowells for isolation of cells
 - ii. Build a novel optical detection platform for real-time quantitative analysis
 - iii. Build a model to illustrate cytokine secretion dynamics from single-cells
- b. Combine the model with the platform to enable answering questions regarding cytokine secretion dynamics.

The platform and tools we will build within this work will enable:

- a. Measuring the dynamics of cytokine secretion from single cells
- b. Understanding the roles of individual cells in collective behavior of cell populations
- c. Constructing models for cytokine secretion dynamics and assessing the effectiveness of these models in describing immune responses
- d. Defining and establishing correlations between the parameters of cell populations using these models

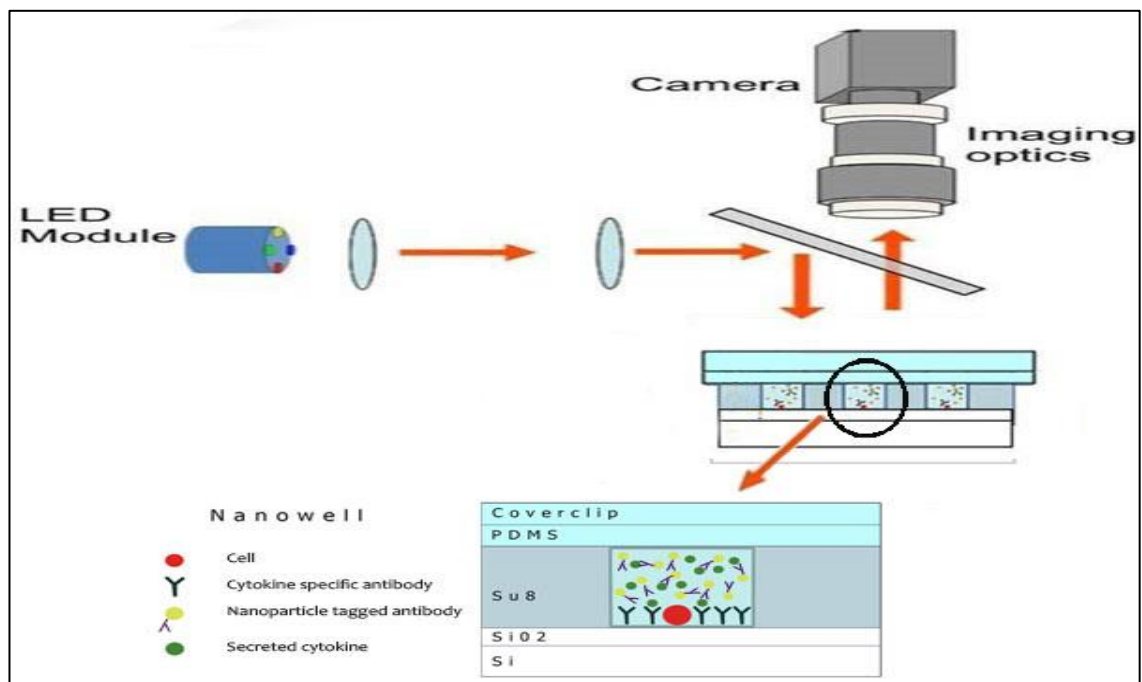
2. OPTICAL DETECTION

2.1 DETECTION APPROACH

The novel methodology proposed in this work for dynamically detecting analytes secreted by single-cells requires an elegant combination of two previously developed techniques (microengraving and SP-IRIS). Figure 2.1 illustrates the schematics of the proposed detection method. The following changes need to be made to the standard methods of microengraving and SP-IRIS:

- Arrays of nanowells need to be fabricated on layered substrate (Si/SiO₂) (in comparison to PDMS wells in microengraving)
- The capture surface needs to be changed to the bottom surface (in comparison to the top surface in microengraving)
- The surface chemistry for decorating the new nanowell configuration of the sensor surface with capture antibodies need to be optimized (as opposed to flat surface in both methods)

Figure 2.1: Optical arrangement of single particle IRIS system

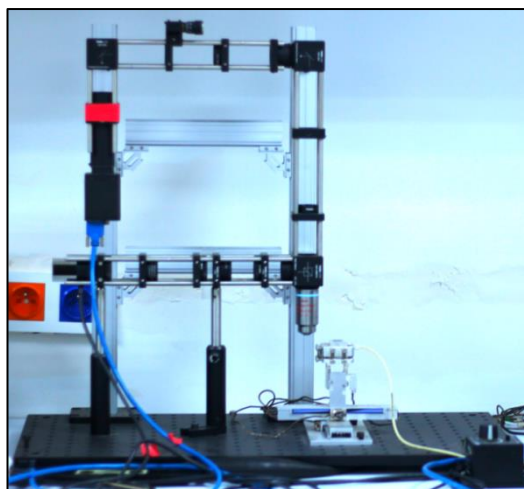


In brief, secretion from cells isolated in nanowells will be captured on the layered substrate. Secondary antibodies tagged with nanoparticles and present in nanowells will bind to the chip surface, and using a high-magnification and high-NA objective, and the sensor surface will be imaged to a CCD camera. Analysis of the image will reveal the presence of nanoparticles due to contrast change at corresponding pixels.

2.2 INSTRUMENT

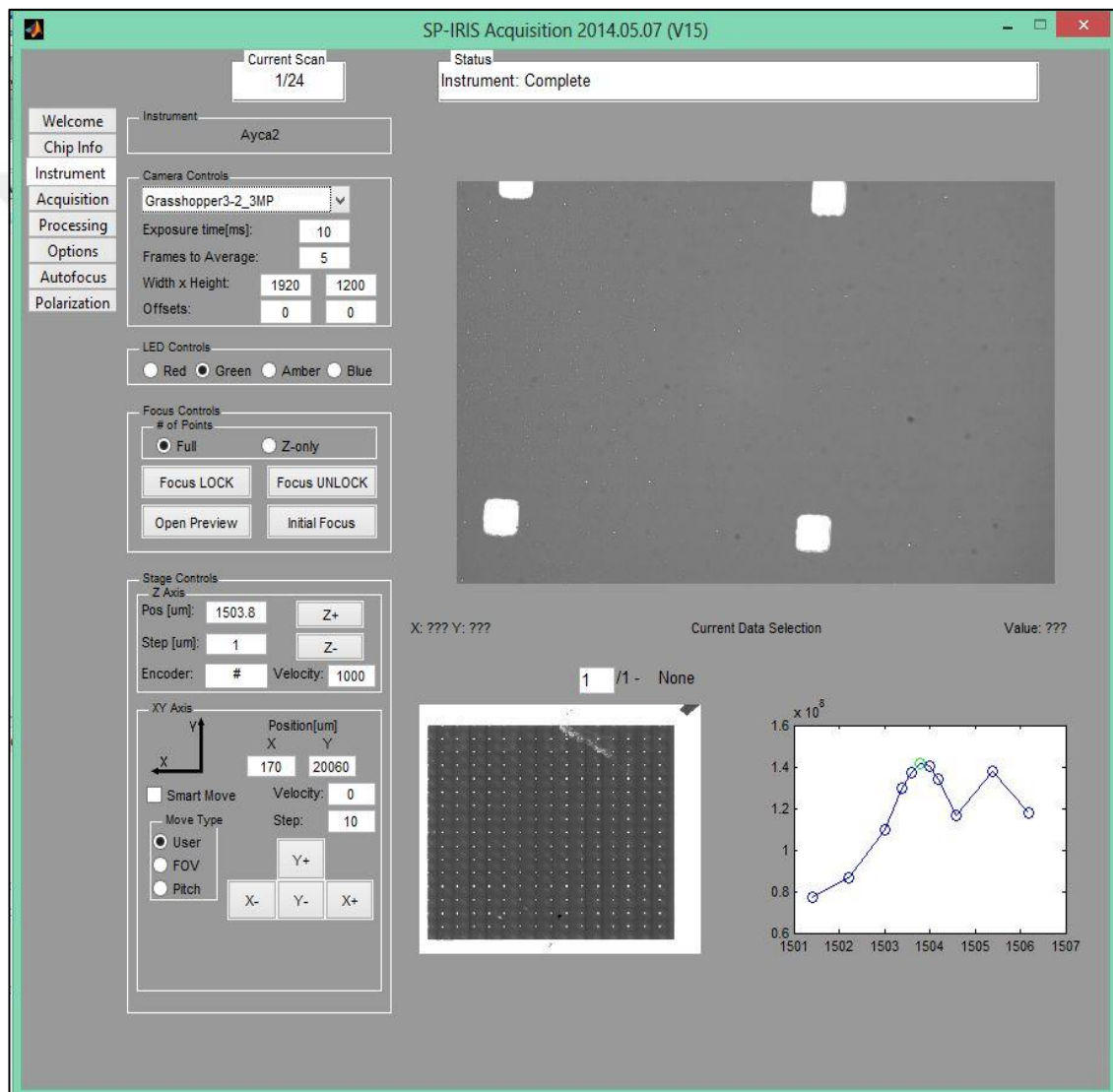
The detection instrument includes a camera (Point Grey – GS3-U3-23S6M-C). This camera has a resolution of 1920 x 1200 with a frame rate of 163 fps and pixel size of 5.86 microns. These features enable good quality high contrast image. The objective has a numerical aperture of 0.8 and allows 50X magnification. For detection of nanoscale particles it gives a field of view of 176.4 x 282.24 microns. The LED illumination source has a central wavelength of 530nm, and is in Kohler illumination configuration. The stage is designed such that it allows mobility in all three axes. For translational movements in x and y axes two position piezo stages (VT-50L) and for movement in z axis an elevation stage (ES-50) were bought from Micronix (USA). The elevation stage has a travel range of 10mm with a resolution of 0.05 micron whereas the translation stages have a closed loop resolution of 50nm with a travel range of 100mm. Figure 2-2 shows a picture of the constructed SP-IRIS setup.

Figure 2.2: The SP-IRIS instrument



We will utilize a previously custom-developed software with a graphical user interface (GUI) that synchronizes the stage, camera and LED control for automated data acquisition and processing (Figure 2-3). The software has a unique image processing algorithm which provides detailed information such as the number of particles, particle size, and distribution.

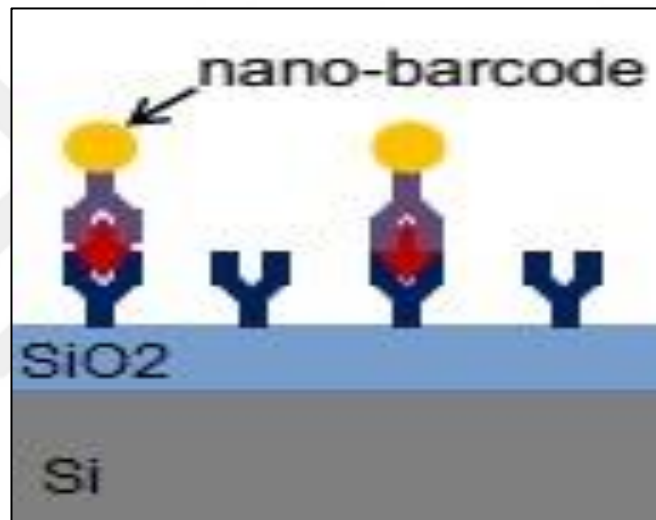
Figure 2.3: The GUI of the acquisition software



2.3 LABELING NANOPARTICLES FOR SINGLE PARTICLE DETECTION

A common method, known as “mass tagging”, for achieving enhanced sensitivity is to label secondary probes with a metallic particle. We will use this approach for detecting captured targets on the surface using SP-IRIS, i.e. by specifically attaching gold or other metallic nanoparticles to the cytokines. We will call the secondary antibody labeled nanoparticles ‘nano-barcodes’, analogous to consumer products each having unique barcode (Figure 2-4), as they will be specific to the cytokine of interest.

Figure 2.4: Detection via nano-barcode feature



2.4 CONCLUSION

Development of biosensors that can simultaneously monitor an array of molecular interactions is of great interest for biomedical research and clinical applications. The detection scheme described in the chapter provides a less complex and cost effective sensor platform for detection real-time secretion of cytokines from single-cells in an array format.

3. NANOWELL FABRICATION

3.1 INTRODUCTION

To isolate the cells for optically detecting the cell-secretions, we need to fabricate nano-environments for the cells that not only allow the isolation of cell but also permit optical monitoring of the isolated cells. This chapter discusses the fabrication process of arrays of nanowells. A mask design of four different well sizes of 50, 70, 100, and 150 microns in width and length was generated and a photo-mask having the customized mask design was created. For photolithography, we used silicon substrates with thermally grown oxide layers of 100nm and a negative photoresist, SU-8 3050. We optimized the lithography process to get 50 micron resist thickness.

3.2 MASK DESIGNS

For creating nanowells on the surface of silicon oxide wafers using lithography, a mask was designed using Autodesk AutoCAD. The mask includes four different designs ultimately giving four different well sizes ranging from 125pL to 1.125nL. Each nanowell array is designed to fit in a 16.5 mm x 16.5 mm final chip size, and the number of nanowells in the array are adjusted accordingly. These designs were then arranged in such a manner to cover the entire mask, where each design can be found in the center and perimeter of the mask.

The first design comprises nanowells of (50 x 50) microns arranged in an array of (2 x 3) wells, repeated in a five column and five rows fashion over the chip (Figure 3-1). The size of each subarray (2 x 3) within the chip is selected to fit maximum number of wells within a single field of view offered by our optical detection system i.e. (176.4 x 282.24) microns. The next design comprises nanowells of (70 x 70) microns arranged an array of (1 x 2) wells as shown in Figure 3-2. The third chip design single wells of (100 x 100) microns per field of view (Figure 3-3), and the final design has single wells of (150 x 150) microns (Figure 3-4).

Figure 3.3: Mask design to create 100x100 micron wells.

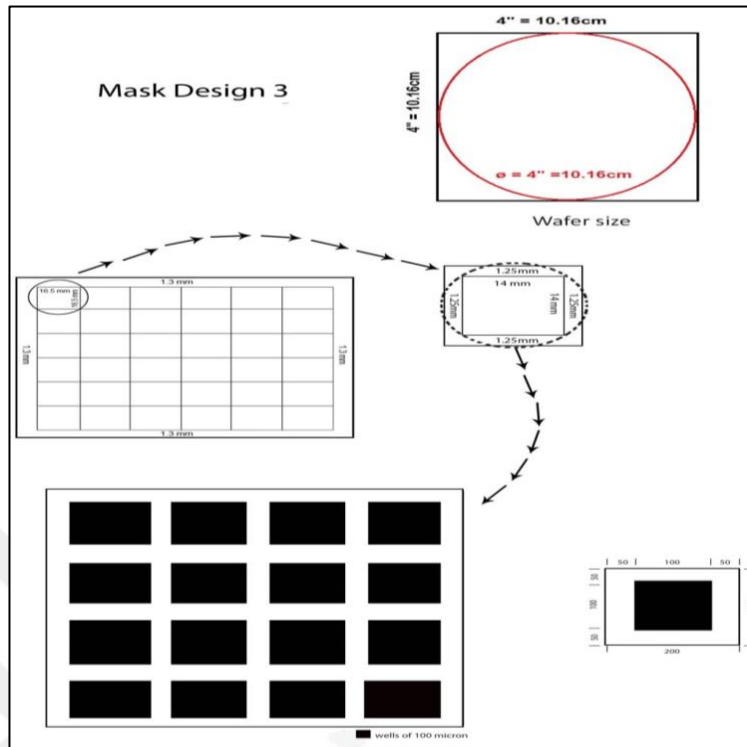
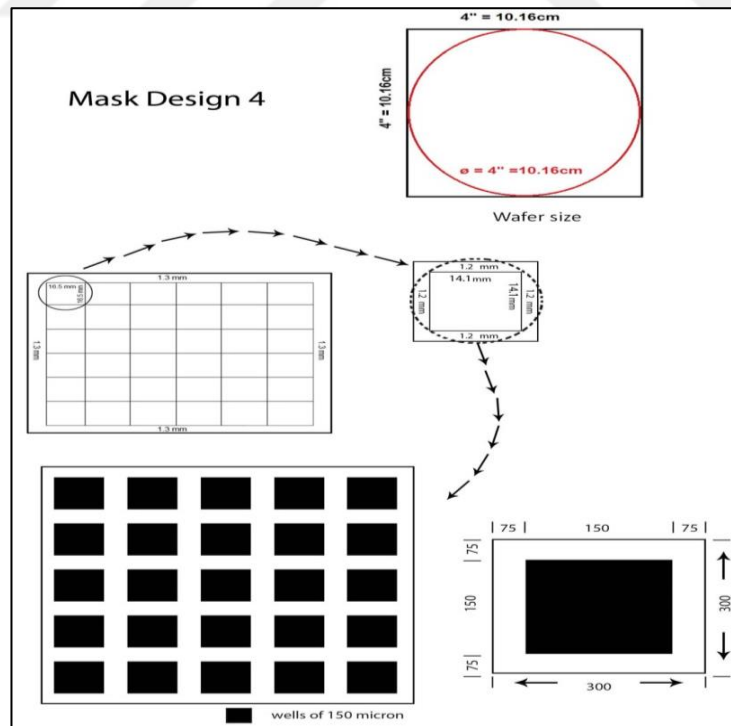


Figure 3.4: Mask design to create 150x150 micron wells.



3.3 FABRICATION PROTOCOL

Silicon wafers of four inch diameter with thermally grown oxide layer of 100 nm thickness were used as substrates. To create nanowells on the substrates, a photoresist polymer is patterned using photolithography. Photolithography also known as optical lithography or UV lithography is a process widely used in microfabrication. The process uses light to transfer a geometric pattern on the substrate. For example, in integrated chip technology, photolithography is used to transfer patterns on the semiconductor wafer. (18).

Initially, the wafer is covered with photoresist by spin coating, the liquid solution of photoresist is dispensed on the wafer and the wafer is spun rapidly to produce a uniformly thick layer. The photoresist coated wafer is then soft-baked or pre-baked to drive off excess solvent. Next the wafer is exposed to UV light through a photo-mask. The photo-mask has been predetermined of the patterns and the shapes of the desired outcome; once the UV light is turned on, the light will go through the transparent areas of the photo-mask and will reach the photoresist layer hence hardening/softening it. The wafer is then dipped in specific developer solution to remove the undesired photoresist (Figure 3-5). For negative photoresist the unexposed areas of the resist will dissolve during the developing step whereas for positive photoresist exposed areas will dissolve in the developing solution.

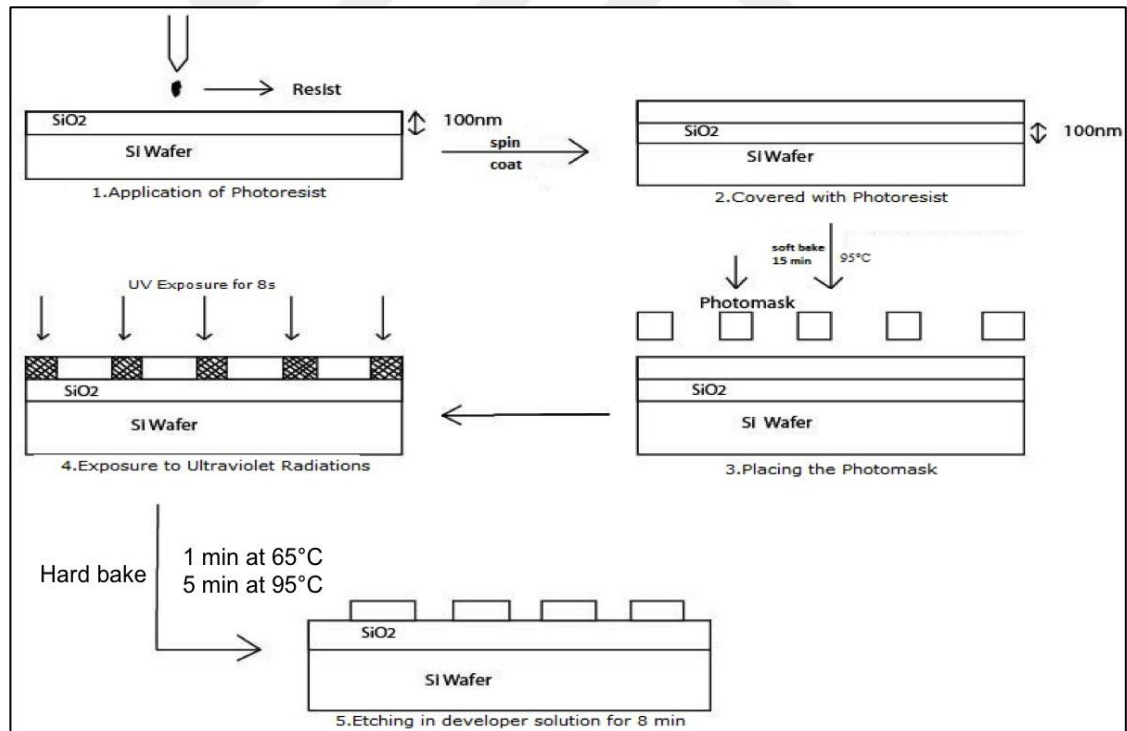
The photoresist, SU-8 (3050), is chosen to provide a uniform thickness of 50 microns. It is a negative photoresist with high optical transmission above 360 nm and has high imaging characteristics, producing very high, over 5:1 aspect ratio structures (19). To create nanowells of 50 micron depth with this photoresist, we have optimized the protocol as the following:

1. Pour approximately 1 mL of SU-8 photoresist per inch diameter on the center of the silicon oxide wafer. (4mL for the 4 inch wafer).
2. For spreading the resist uniformly over the entire surface of the silicon oxide wafer, spin coat the wafer initially at 500 rpm for 7 seconds at an acceleration of

100 rpm/s; to cover the entire wafer surface with the resist, followed by another spin cycle at the same acceleration for 45 s increasing the speed to 2500 rpm; to create a uniform thickness.

3. Soft bake the wafer on a hot plate at 95°C for 15 min.
4. Place the wafer under the hard mask in a mask aligner and expose with UV light intensity of 23 mW/cm² for 8 seconds.
5. Bake the wafer initially at 65°C for 1 min followed by 95°C for 5 min.
6. Immerse the wafer in the developer solution for 8 min so that the unexposed resist dissolves in solution.
7. Rinse with the developer and Isopropyl Alcohol (IPA), and dry the wafer with nitrogen gas.
8. Dice the wafer according to the chip sizes required.

Figure 3.5: Steps of fabrication

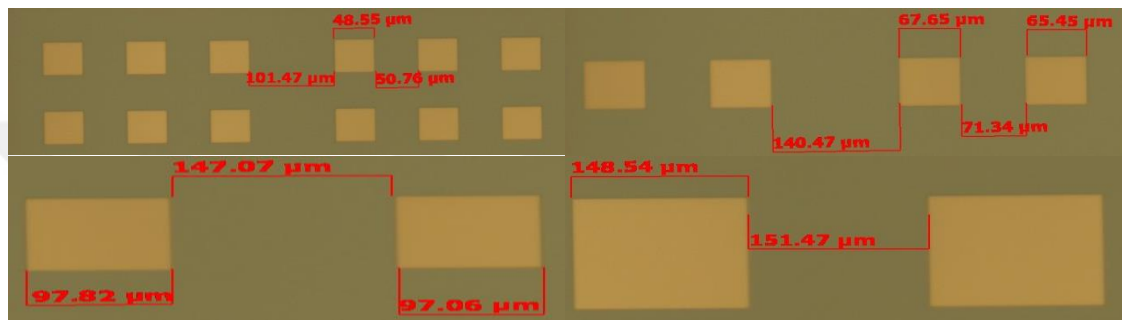


3.4 POST-FABRICATION RESULTS

The whole micro-fabrication process was conducted in the clean room of Sabanci University's Nanotechnology Research and Application Center (SUNUM). After a

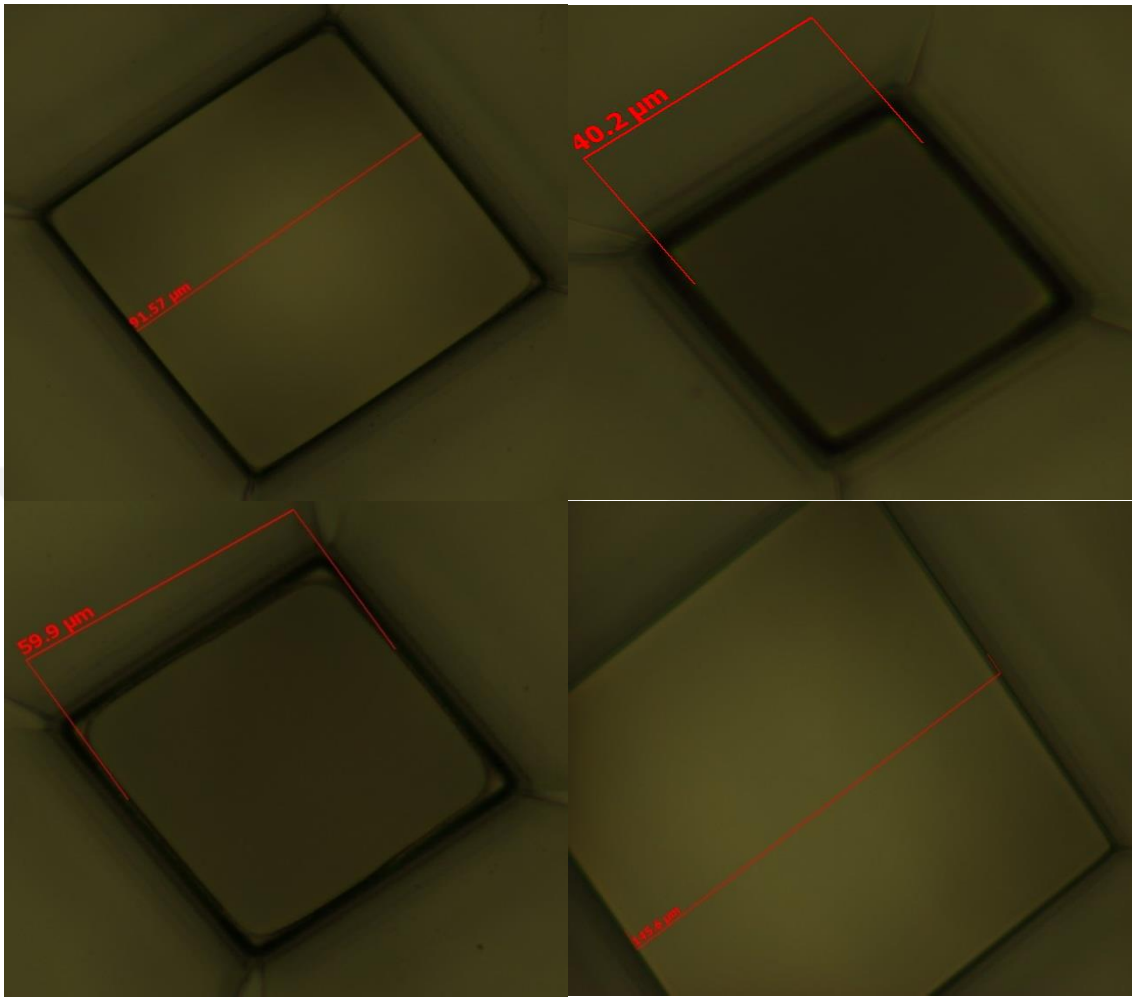
safety training, authorized access to the clean room was granted. The hard mask was prepared by the clean room expert, whom we provided our customized design layout. Since a negative photoresist was chosen, the mask was created to allow the unexposed area to dissolve during the developing step i.e. the mask was fabricated using e-beam lithography with well areas (chromed). The dimensions of the mask designs were verified after fabrication using a microscope (Figure 3-6).

Figure 3.6: Post-fabricated mask with labeled dimensions of all four mask designs.



The photolithography protocol stated above was carefully followed to fabricate the well arrays over the SiO₂ wafer. The lateral dimensions of the fabricated wells were verified using a microscope, and illustrates successful fabrication of the arrays (Figure 3-7).

Figure 3.7: Post-fabrication-microscope images (50X) displaying dimensions of well-sizes.



The depths of the wells were then verified using a profiler. The resist thickness for the (150 x 150) micron wells is measured to be 58 microns (Figure 3-8). The well-depths were analyzed for each well design fabricated, and we observed a non-uniformity for well sizes smaller than 150 microns (Figure 3-9).

Figure 3.8: Post fabrication profiler results measuring resist thickness of (150x150) wells to be 58 microns.

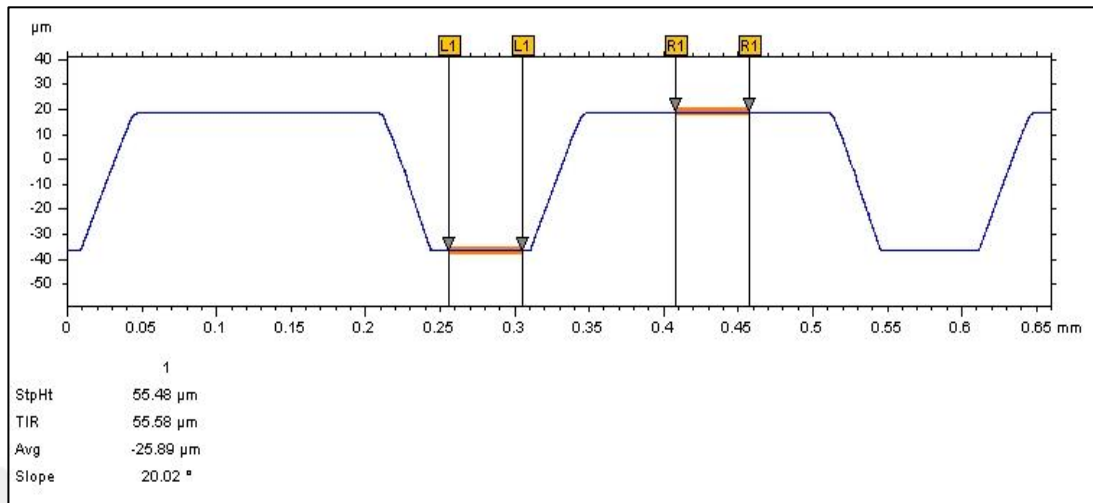
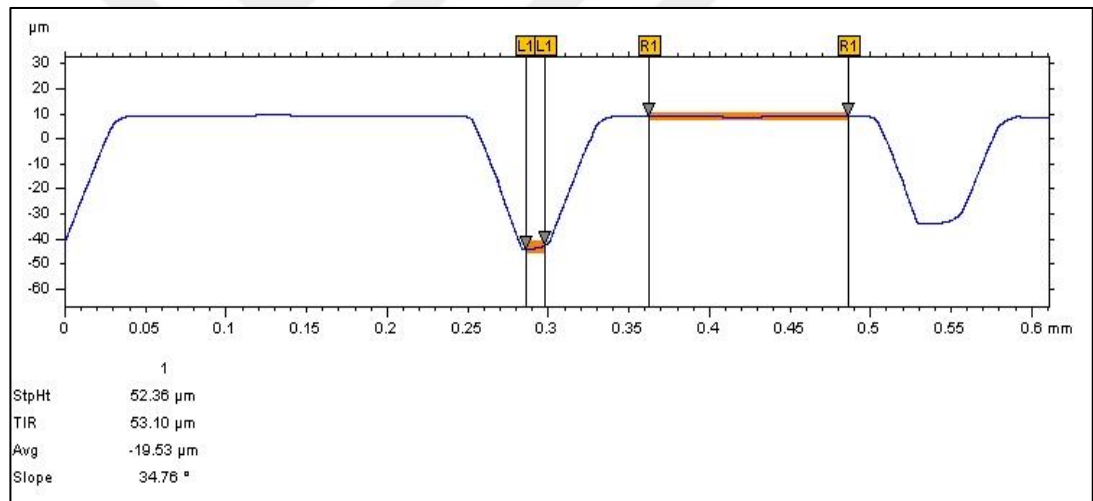


Figure 3.9: Profiler measurements for well-depth of the 100 micron nanowell array



To overcome the non-uniformity of the well depth, we tried to optimize our fabrication protocol. Initially, it seemed that the 50 µm wells are not completely developed, that is the 50µm wells still have some resist left (Figure 3-10). Therefore, we started the modification of our protocol by increasing the developing time, and re-developed the same wafer for another 5 minutes (Figure 3-11). An increased well depth was observed however the uniformity of the well depth throughout the array was still visible.

Figure 3.10: Profiler measurements for the 50 micron wells. A non-uniform well depth is observed.

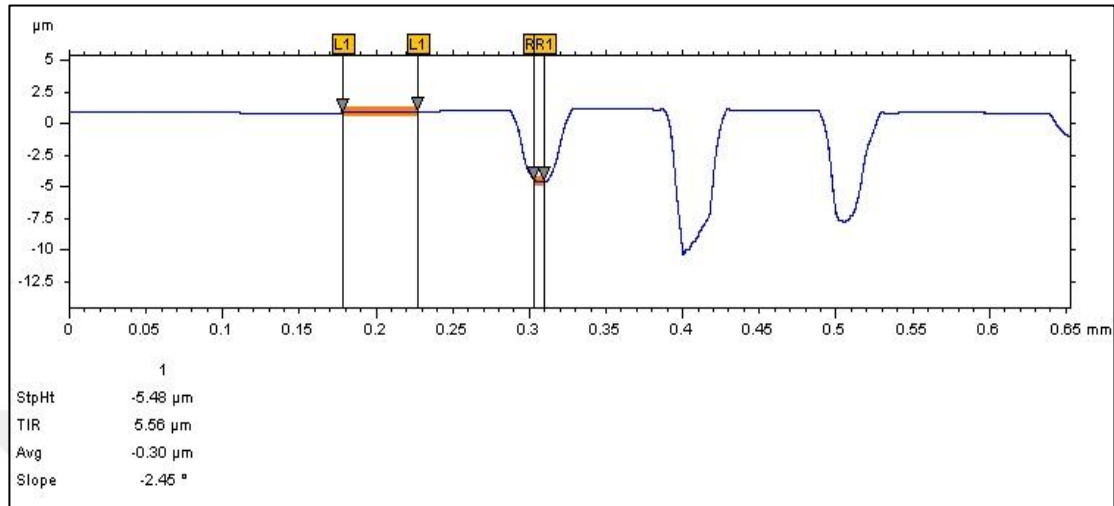
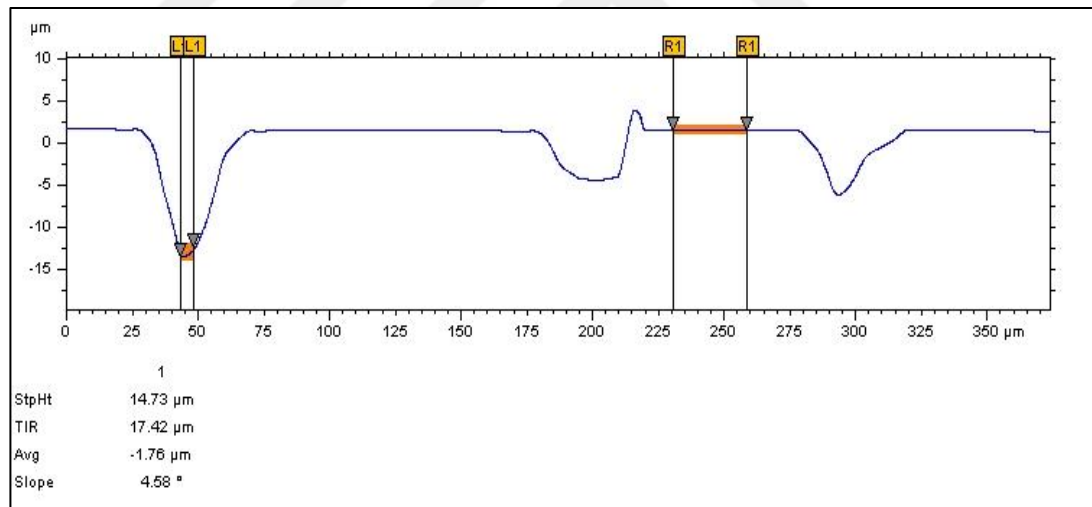


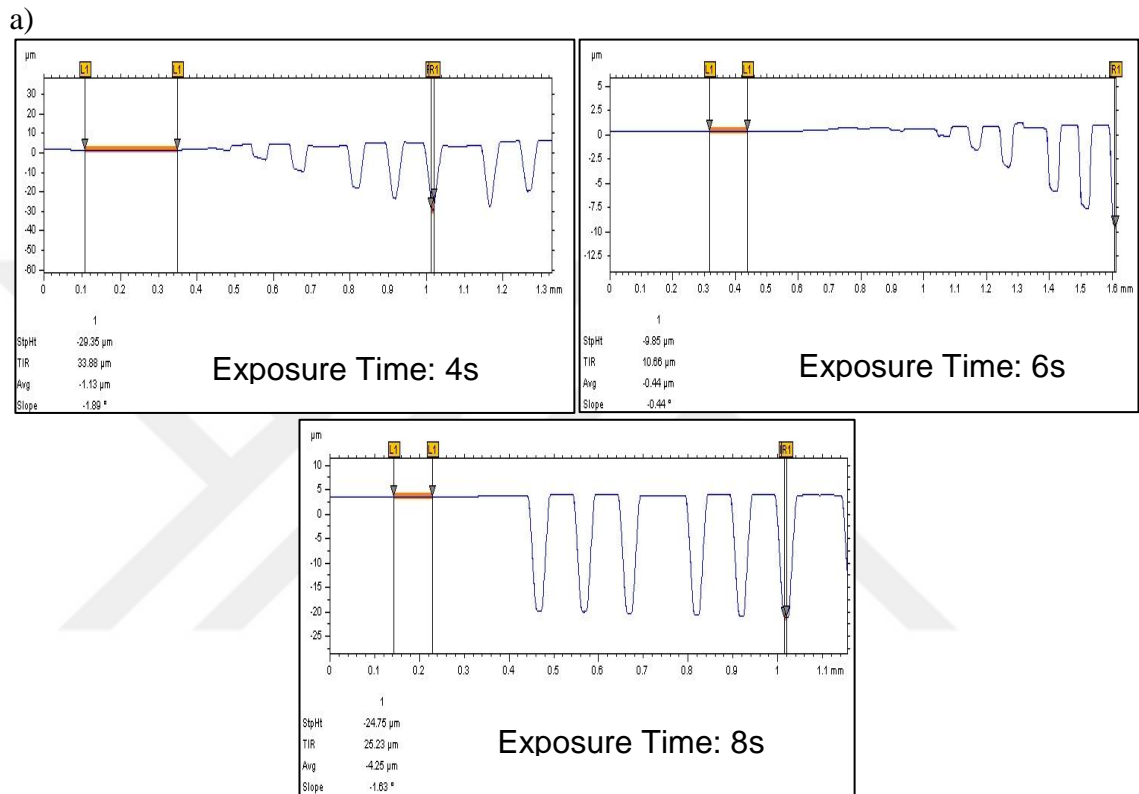
Figure 3.11: Profiler measurements for the 50 micron wells after increasing developing time. The non-uniformity in well depth is still visible.



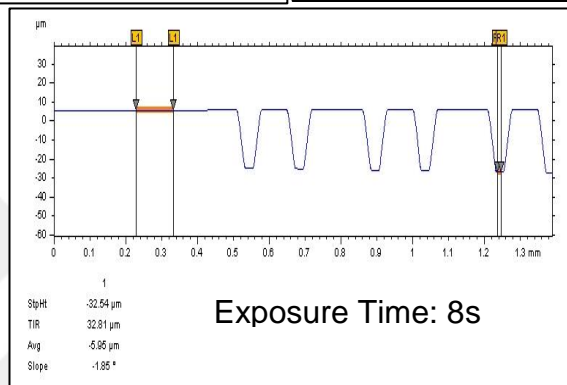
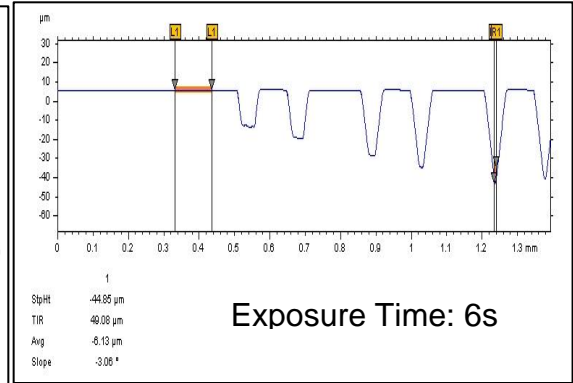
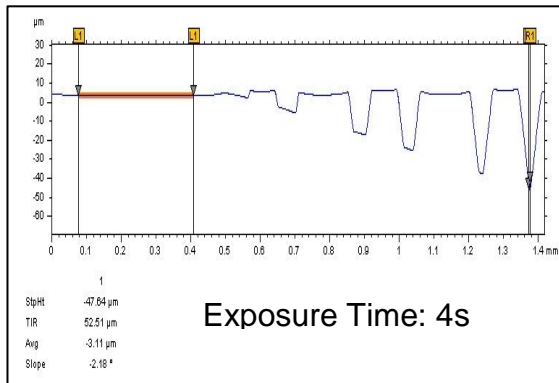
We were using the proximity contact method for UV exposure, i.e. there was a gap of 2-5 microns between the mask and the substrate, and it seems that prolonged UV exposure caused penetration of light towards the side walls of the exposed areas, influencing the unexposed areas, and thereby creating non-uniformity in well-depths. Therefore, as a second step in the revision of the fabrication protocol, since the mask aligner does not offer any alteration in UV light intensity, the UV exposure time was altered. We have applied UV exposure of 4, 6, and 8 seconds on three different wafers and developed

each for 8 minutes. The results acquired using the profiler shows best uniformity with 8 seconds exposure time for all the well sizes (Figure 3-12). Thus, we reduced the UV exposure time from 12 seconds to 8 seconds.

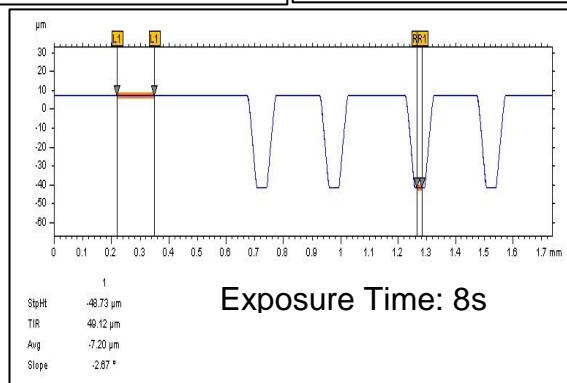
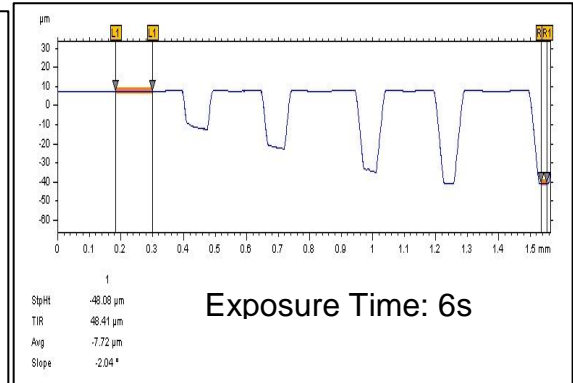
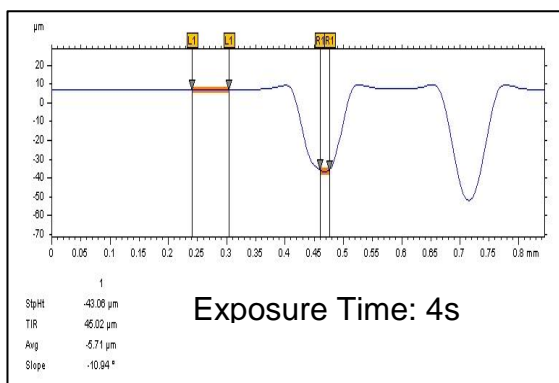
Figure 3.12: Profiler measurements for 4,6 and 8 seconds of exposure time. a) 50x50 micron wells, b) 70x70 micron wells, c)100x100 micron wells



b)



c)



3.5 DISCUSSION AND CONCLUSION

Chips with nanowell arrays that will allow optical detection of cytokines in real-time have been successfully fabricated. After initial tests, the compatibility of the wall material (SU-8) with the cells need to be tested through viability studies. Other materials with increased biocompatibility will be tested if necessary.

The functionalization of the nanowell arrays is not as trivial as the functionalization of flat glass surfaces. The use of 2-dimensional and 3-dimensional surface chemistries with these arrays for surface activation, and effective immobilization of capture antibodies needs to be tested.

Finally, we will add reference marks and numbers to the next generation mask designs for locating any specific nanowell during measurement and analysis more easily and for quick access to information related to well size.

4. NUMERICAL SIMULATIONS OF THE NANOWELL SYSTEM

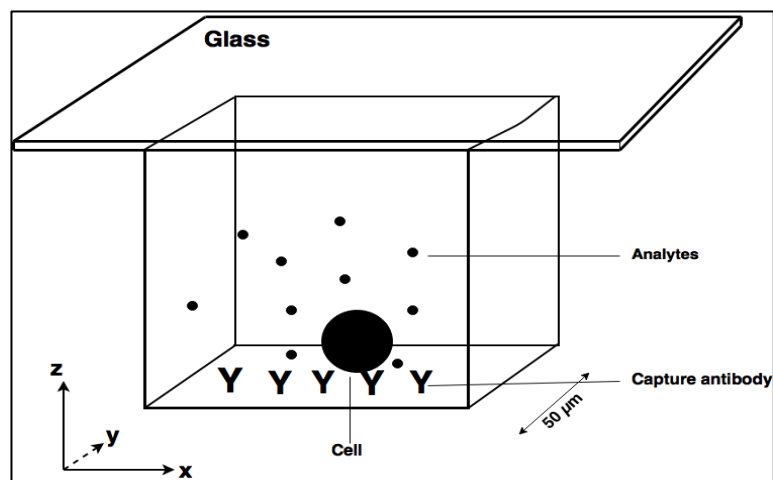
4.1 DEFINING THE MODEL

We have developed a numerical model for the secretion of analytes from single cells inside nanowells and their capture on the sensor surface. The numerical model includes the secretion of analytes from the cell, the diffusion of the analytes in the nanowell volume and capture on the reaction surface decorated with antibodies with specific affinities for the secreted analytes.

4.1.1 Physical Model

The model geometry is a well in cubic form with dimensions $(50 \times 50 \times 50) \mu\text{m}$, $(70 \times 70 \times 50) \mu\text{m}$ and $(100 \times 100 \times 50) \mu\text{m}$. The base is silicon oxide, the four sidewalls are SU-8 and the top surface is a glass coverslip (Figure 4-1). Initially, we consider the simplest model, i.e. the isolated cell secretes only one type of analyte, the reaction surface (bottom of the well) is occupied by antibodies specific for the secreted analyte, and the analyte secretion rate is not affected by the analyte concentration within the well.

Figure 4.1: Schematics of a nanowell containing a single cell



4.1.2 Assumptions for simplification of the model

Three assumptions were made to ease the numerical simulation and to simplify the model.

1. The airtight nanowell system had neither liquid or gaseous inflow nor outflow. The analytes are only transported via diffusion.
2. Rate of secretion (k) of the isolated cell in the nanowell system remains constant at all times.
3. Permeability and adsorption of analytes on the SU-8 walls is considered to be negligible.

The secretion rate depends on various factors such as the type of cell isolated in the nanowell system, the quality of environment in the nanowell, the ability of the cell to secrete, and its state in the cell cycle. Regardless, the assumption of a constant secretion rate remains worthy in this model to understand the secretion dynamics between the number of analytes released and the amount of analytes bound on the bottom reaction surface at any point in time.

4.2 MATHEMATICAL EQUATIONS

The total amount of analytes released from the isolated cell in the nanowell increases proportionally with time.

$$N = kt \quad (\text{Eq. 4})$$

where, N (**molecules**) is the total number of analytes secreted from the cell, k (**molecules/s**) is the rate of secretion, and t (**s**) incubation time.

For N to be implemented in the simulations, it was required to use the moles of analytes secreted from the unit cell surface area, therefore convert the unit to mol/m^2 . In this case, N used in simulations becomes:

$$N = \frac{k}{N_a \cdot 2 \cdot \pi \cdot (r^2)} * t \quad (\text{Eq. 5})$$

where, N_a is Avagadro's number = 6×10^{23} molecules/mole and $2\pi r^2$ is the area of cell hemisphere with radius r .

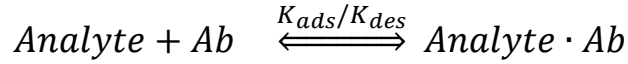
To define the diffusion of analytes from the secreting cell and its capture on the functionalized bottom surface, the model uses two equations, respectively.

The diffusion equation of the analytes inside the volume of a closed well is

$$\frac{\partial C}{\partial t} - D \nabla^2 C = 0 \quad (\text{Eq. 6})$$

where, C (mol/m^3) is the concentration of analyte in the nanowell, and D (m^2/s) is the diffusion coefficient of the analyte.

A reversible process that defines the dynamics of the analyte-antibody pair on the bottom reactive surface is:



Therefore, the boundary condition describing the adsorption and desorption reactions of the analytes on the active surface is:

$$\frac{\partial C_s}{\partial t} = K_{ads} \cdot C \cdot (\delta_s - C_s) - K_{des} \cdot C_s \quad (\text{Eq. 7})$$

where, K_{ads} ($\text{m}^3 \text{s}^{-1} \text{mol}^{-1}$) is the rate of association/adsorption, K_{des} (s^{-1}) is the rate of dissociation/desorption, C_s (mol/m^2) concentration of the analyte-antibody pair on the active surface, δ_s (mol/m^2) is the density of total binding sites on the active surface, and $(\delta_s - C_s)$ is the density of unbound sites available on the active surface.

Initially, the concentration of the analyte in solution and on the surface is zero, i.e. at time $t=0$, $C=0$, $C_s=0$ and $\delta_s=\delta_s$. The values of parameters used in the numerical simulation are listed in *Table 4.1*.

Table 4.1: Values of the parameters used in simulations

| Parameters | Value |
|--|--|
| Well size | (50 x 50 x 50) μm |
| Cell radius (r) | 5 μm |
| Association/adsorption rate constant (K_{ads}) | $10^2 \text{ m}^3 \text{ mol}^{-1} \text{ s}^{-1}$ |
| Dissociation/desorption rate constant (K_{des}) | 10^{-5} s^{-1} |
| Secretion rate (k) | 10 s^{-1} |
| Diffusion coefficient (D) | $3 \times 10^{-11} \text{ m}^2 \text{ s}^{-1}$ |
| Density of total binding sites (δ_s) | $10^{-9} \text{ m}^{-2} \text{ mol}$ |

4.3 RESULTS

The partial differential equation corresponding to secretion, diffusion, and binding of analytes with specific antibody were solved in COMSOL Multiphysics 5.0 (COMSOL Inc., Stockholm, Sweden). The results gave three-dimensional concentration contour maps of analyte in the nanowell as a function of time. Using the simulation tool, two dimensional model geometry was constructed to visualize the heat map of the concentration distribution in the entire volume of the well (Figure 4-2).

For each time point, we calculated the total number of analytes in the cubic volume, and the antibody-analyte concentration on the bottom surface (Figure 4-3). The dynamics of the results may be explained in three time regimes:

1. At time $t=0$, the number of analytes inside the nanowell starts increasing, and the analytes start binding to the bottom surface rapidly as the molecules quickly diffuse to the nearby bottom reaction surface.
2. After approximately 30 minutes (for a secretion rate of 10 molecules/s), the rate of binding of analytes to the bottom surface is lowered as the density of the

available binding sites is lowered. At this point, the number of analytes inside the nanowell starts increasing at a faster rate.

3. Ultimately, an equilibrium is reached between the amount of analytes and the available binding sites on the active surface ($C_s \sim \delta_s$). At this point in time (~22 hours) the analytes bound on the surface reaches a steady-state, and the number of analytes inside the nanowell starts increasing with a rate approaching the rate of secretion.

Figure 4.2: Heat map to visualize concentration distribution in volume using same physical parameters as shown in Table 4.1. Total incubation time is 30 hours.

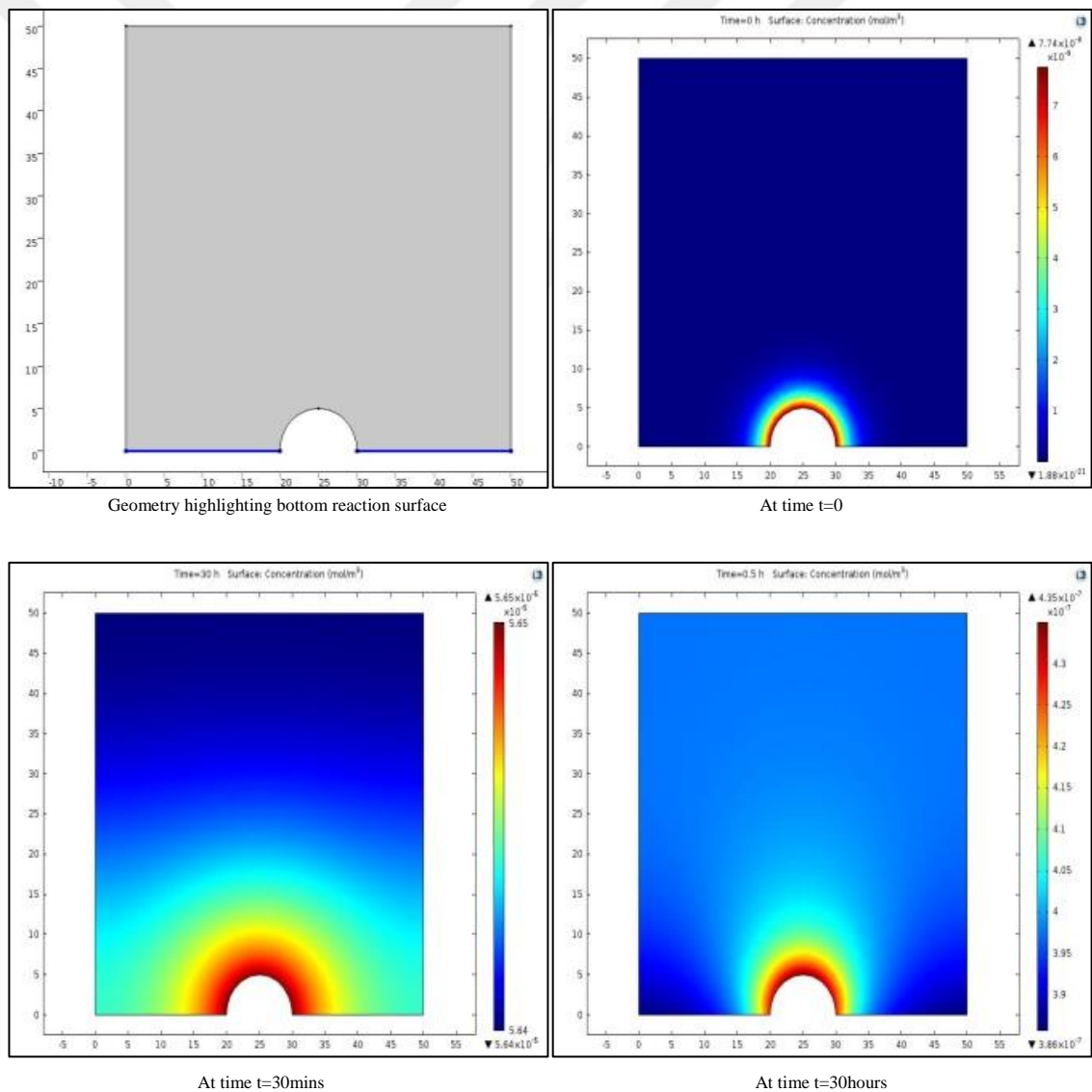
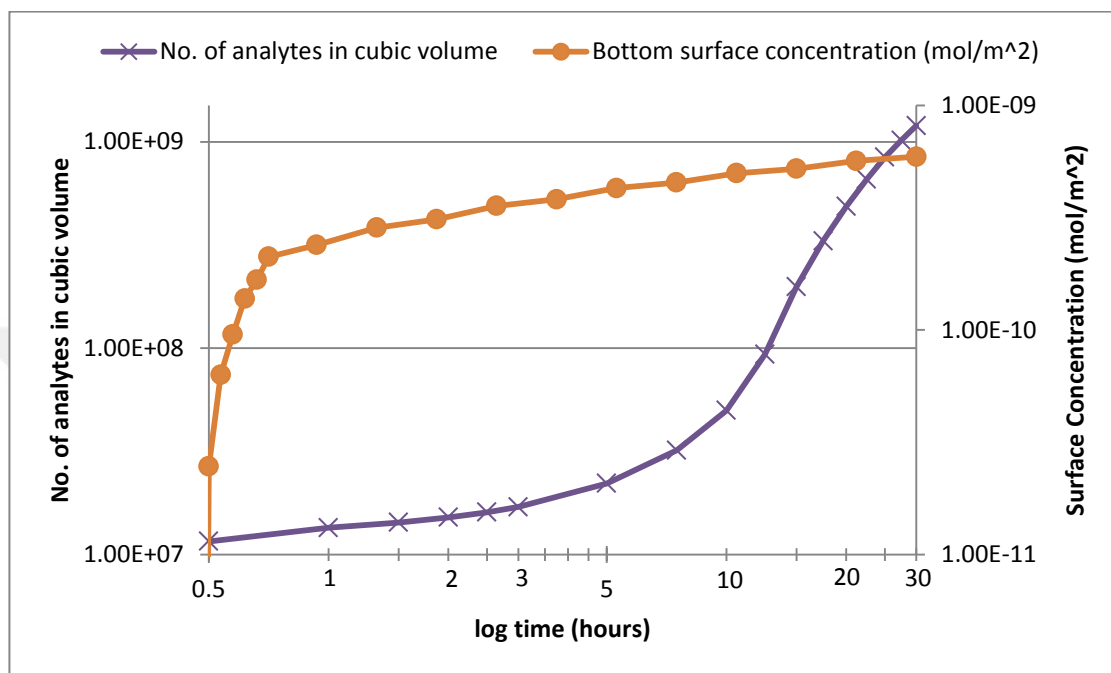


Figure 4.3: Plots of the calculated quantity of analytes accumulated in nanowell and on the bottom surface during microengraving when the cell secretes at a constant rate of 10 molecules/s.



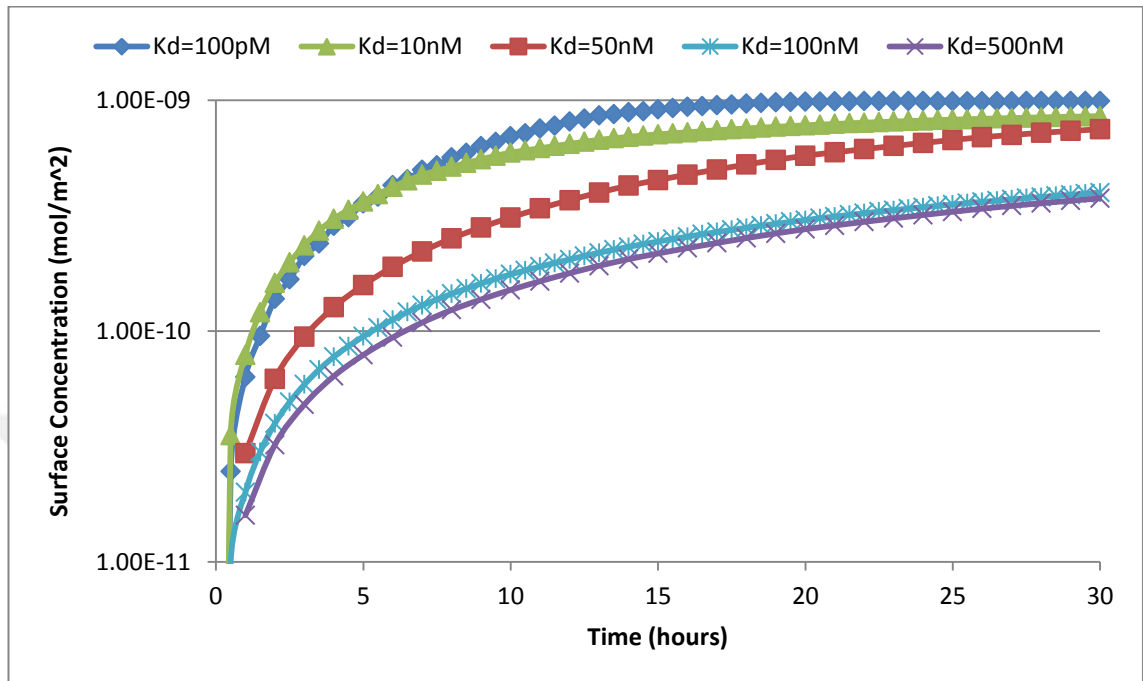
4.4 EFFECTS OF MODEL PARAMETERS ON SIMULATION RESULTS

The influence of critical system parameters on the simulation results have been investigated, and the results are discussed below:

4.4.1 Effect of the Equilibrium Dissociation Constant (K_D)

The ratio of K_{des}/K_{ads} between the antibody and its antigen is called the Equilibrium Dissociation Constant (K_D). For antibodies with higher affinity, e.g. $K_D \sim 10^{-10}$ M, the number of analytes secreted during incubation almost equals to the number of analytes bound on the active reaction surface ($95-99\% N_{total} \sim N_{surface}$) (Qing Han, 2012). Figure 4-4 shows the effect of K_D on the surface-bound analyte concentration for $K_D=100$ pM, 10nM, 50nM, 100nM and 500nM. As expected, as K_D increases, the capture efficiency is lowered. For values below 50nM, the surface concentration that builds up within a couple of hours is lowered significantly.

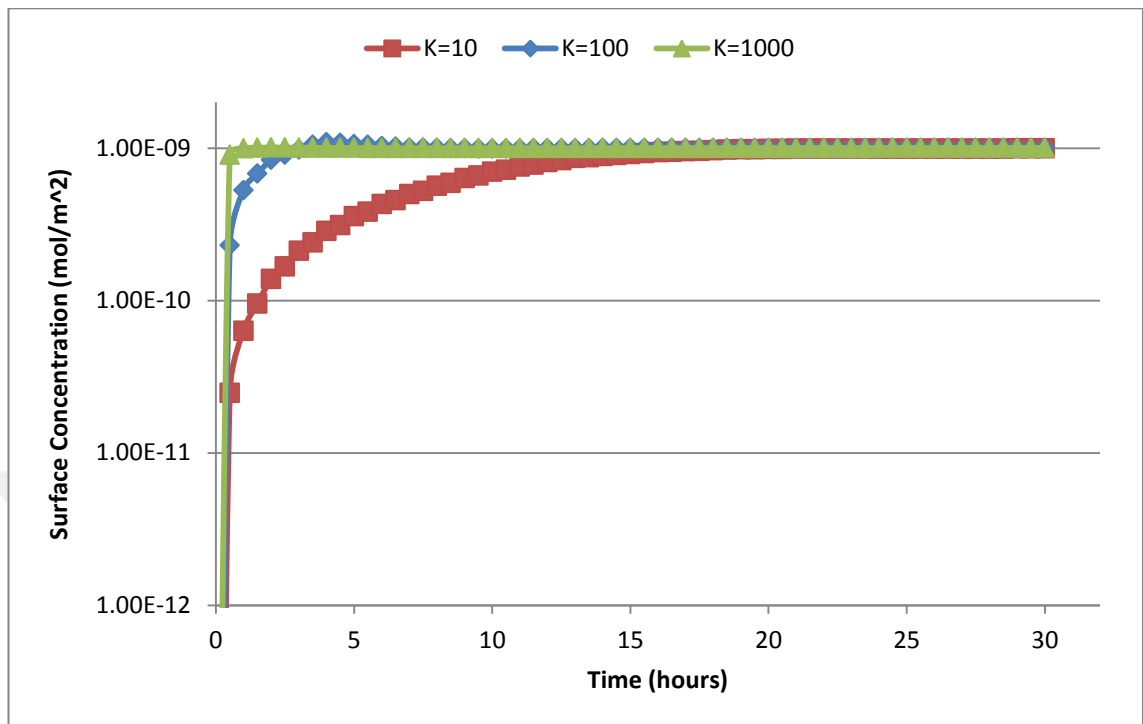
Figure 4.4: Graph showing decrease in surface concentration with the increase in K_D



4.4.2 Effect of Rate of Secretion (k)

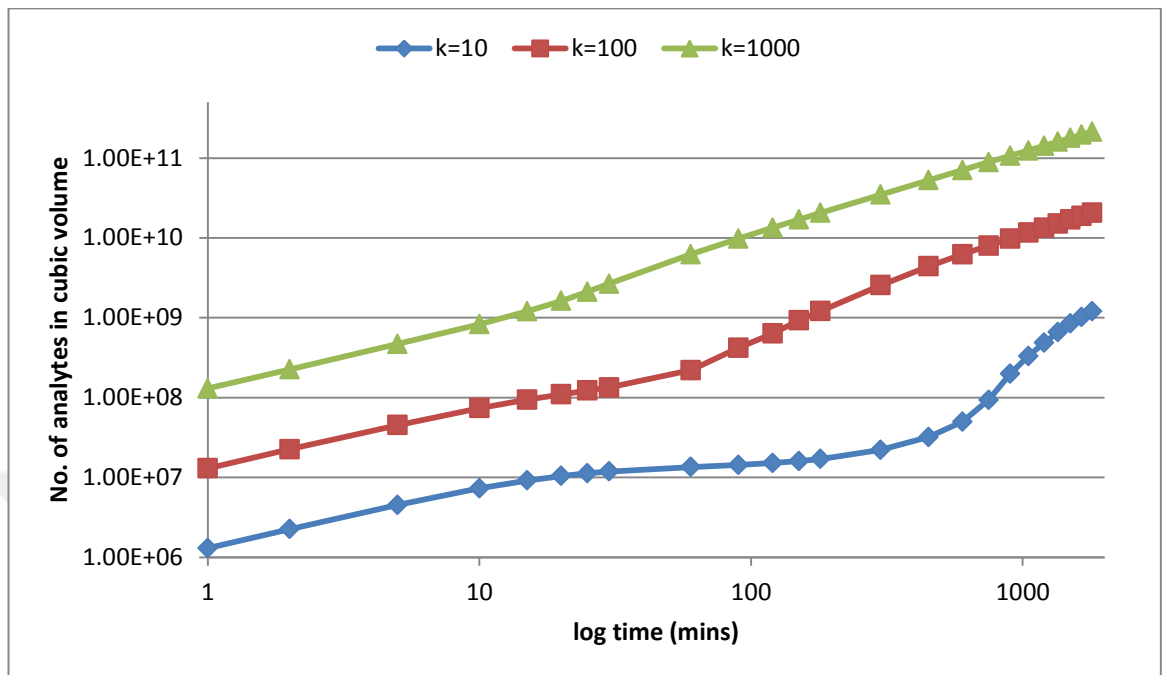
Simulation results indicate that with the increase in secretion rate, the binding rate of secreted analytes with available antibodies on the active surface increases, eventually saturating the bottom reaction surface (Figure 4-5). As expected, as k increases, the time-to-saturation of the reaction surface is decreased. For $k=100$ molecules/second, the reaction surface is saturated at approximately 3 hours, where all the binding sites on the reactive surface are occupied.

Figure 4.5: Graph shows surface concentration saturation trend with the increase in secretion rate



Overall, the increase in number of analytes present in the enclosed nanowell starts as soon as the bottom reaction surface gets saturated. Initially, from $t=1$ mins to $t=30$ mins there is a linear increase in number of analytes in the volume of the nanowell. The result clearly explains the linear increase in secretion rate is affected during the period when analytes are binding with antibodies present on the active surface (Figure 4-6).

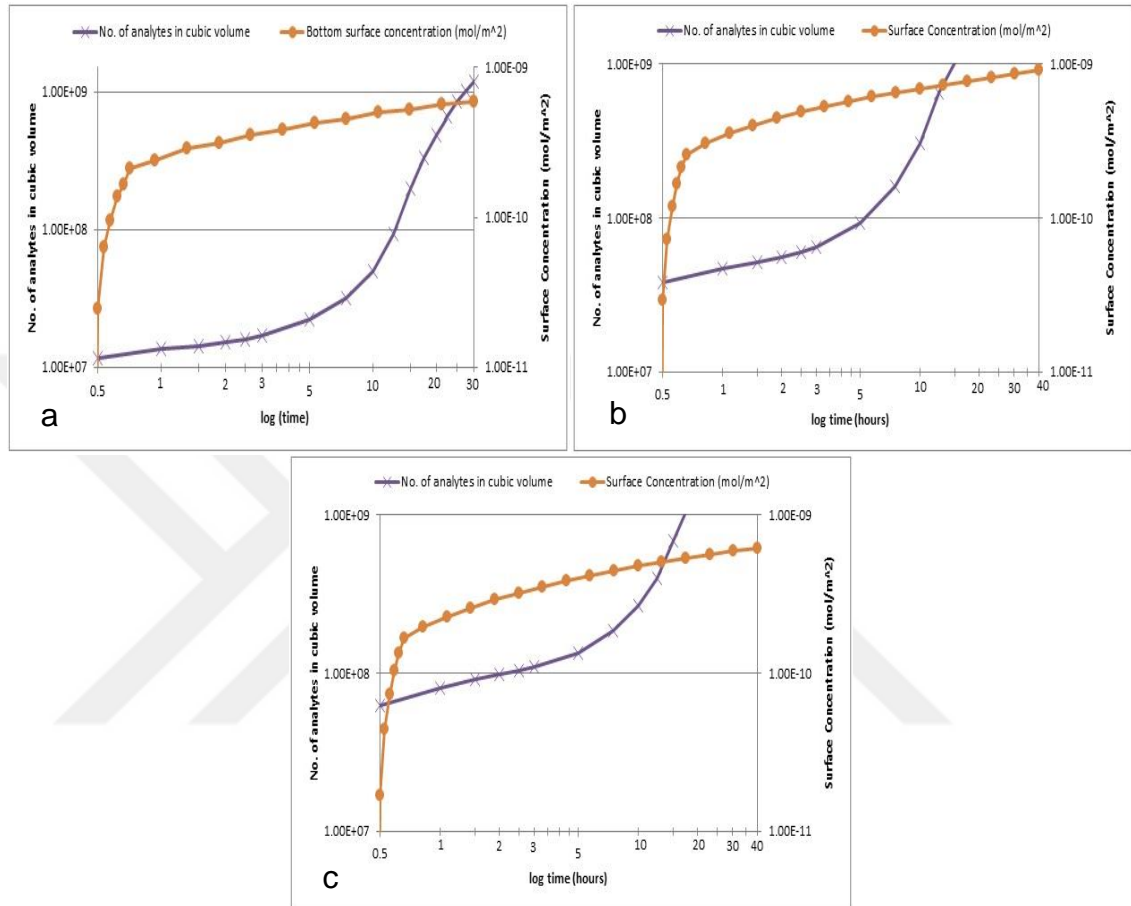
Figure 4.6: Graph illustrates trend of increase in number of analytes in cubic volume with the increase in secretion rate (k)



4.4.3 Effect of Nanowell Size

Geometric parameters, such as the size and shape of the nanowell and even the position of the cell in the nanowell impact the distribution of secreted analytes. To illustrate the effect of nanowell size, we repeat the simulations with well sizes of (70x70x50) microns and (100x100x50) microns. The time for the active surface to get saturated is increased as expected due to increase in well size so we increased our incubation time from 30 hours to 40 hours (Figure 4-7b). For well size of 100x100 microns the saturation of the bottom surface takes even longer than 40 hours (Figure 4-7c).

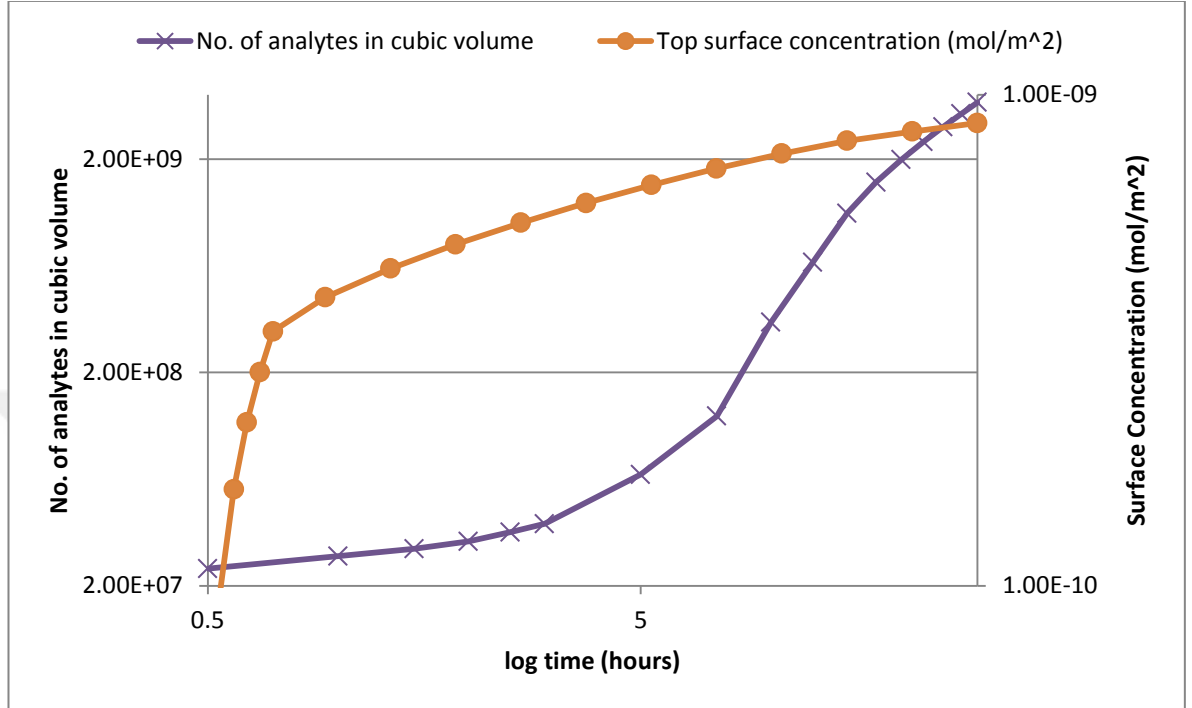
Figure 4.7: Plot showing the number of analytes accumulated in the nanowell and on the bottom surface during microengraving using same parameters as in Table 4.1 except (a) well size of (50x50x50) μm with cell being incubated for 30 hours (b) well size of (70x70x50) μm (c) (100x100x50) μm , with cell being incubated for 40 hours.



4.4.4 Effect of the Position of the Reaction Surface

We switched the top glass surface to the active reaction surface, keeping all the parameters same as mentioned in Table 4.1. There was not much difference visible by the numerical results and the entire process involves the same three temporal regimes (Figure 4-8). However, for analytes to complete occupy all the available binding sites on the top glass surface increases to approximately 27 hours.

Figure 4.8: Graph showing the number of analytes in nanowell and on the glass surface positioned on top when the cell secretes 10 molecules/s with a dissociation constant $K_D=100\text{pM}$ and density of binding sites of 10^{-9} mol/m^2 .



4.5 DISCUSSION

The numerical simulations have been successfully completed to reflect interactions of the secreted analytes in nanowells with capture surfaces. Comparisons of simulation results with sets of well-designed experiments will enable testing different models, changing model parameters, as well as defining new ones. We can modify our basic model by making simple modifications such as adding feedback as shown in Equation 8. The continuous model may then have the form:

$$\frac{dC}{dt} = s + F(C(t - \tau)) - G(C(t)) \quad (\text{Eq. 8})$$

Where, $C(t)$ is concentration of cytokine at time t , s denotes basal (constant) secretion rate, $F(C(t - \tau))$ represents self-amplification of secretion, such that the rate of secretion at time t is some (increasing) function of cytokine concentration at time $t - \tau$ with a delay

time τ , and $G(C(t))$ designates rate of uptake and denaturation of extracellular cytokine. We can further test the effectiveness of different functional forms for each term by fitting corresponding models to time series data, and estimating the goodness-of-fit.



5. CONCLUSION

Understanding and interpretation of the human immune system and its response to diseases requires sophisticated techniques for uncovering the diversity of human immune cells and their behavior. Continuous monitoring of individual constituent cells of this network will enable us to better understand the functional variances among the various immune cells and how they interact with one another to raise an immune response.

Conventional analytical measurements assess the functional behavior of the cells only at discrete intervals of time- a major limiting factor. Various techniques such as intracellular staining, enzyme linked immunosorbent spot, biocarbode assay and digital ELISA fail to provide multiplex and multi-dimensional information regarding the single cell behavior in real-time and the interactions between the individual cells affecting the collective response of the cell populations.

In this thesis, a novel platform is designed to enable the quantitative and real time analysis of cytokine secretion from single cells, a method of cell-to-cell communication.

For isolation of single cells, we utilized a method called micro-engraving, which employs a microfabricated array of sub-nanoliter volume wells. Cells introduced over the array of nanoliter wells settle down into each container via gravity and are covered with coverslip hence creating microenvironment for individual cells. To reveal the dynamics of cytokine secretion we used the principles of the Interferometric Reflectance Imaging Sensor (IRIS) for optical detection of cytokines captured in nanowell arrays. We have constructed a numerical model for simulation of cytokine secretion and apture within nanowells. Experimental data obtained from the detection system will enable characterizing the dynamics of the cytokine secretion and the effectiveness of the developed model in explaining individual and collective cell secretions.

REFERENCES

1. Byrd, J.C. (2001). Rituximab Shows Activity in B-cell Chronic Lymphocytic Leukaemia." *Inpharma Weekly* : 2153-164.
2. Thompson, M. (2010). *ImmunoAnalysis- Basic Principles of ELISA*. London: Royal Society of Chemistry.
3. Enzo Life Sciences. (2009). *Immunoassays – ELISA kits. Product Guide*, 5-6.
4. Lequin, R. M. (2005). Enzyme Immunoassay (EIA)/Enzyme-Linked Immunosorbent Assay (ELISA). *Clinical Chemistry*, 280-285.
5. Gebauer, B. D. (2002). Evolution of the enzyme-linked immunosorbent spot assay for post-transplant alloreactivity as a potentially useful immune monitoring tool. *Am J Transplant*, 857-866.
6. Smith, J. (2001). Development and validation of a gamma interferon ELISPOT assay for quantitation of cellular immune responses to varicella-zoster virus. *Clinical Diagnostic Laboratory Immunology*, 871-879.
7. Rinnisland, F. T. (2000). Granzyme B ELISPOT assay for ex vivo measurements of T cell immunity. *J Immunol Methods*, 143-155.
8. Cellular Technology Limited. (2008). *How ELISPOT Assays Work: ImmunoSpot Platform for ELISPOT, Bacterial Colonies, and Viral Plaque. Protocols*.
9. BD Biosciences Research. (2012). *Intracellular Flow. Research Application. Techniques*.
10. Kater, S. B. and Nicholson C. (1973). *Intracellular Staining in Neurobiology*. New York: Springer-Verlag.
11. Ogunniyi, A. O., Story, C. M., Papa, E., Guillen, E., and Love, J. C. (2009) Screening individual hybridomas by microengraving to discover monoclonal antibodies, *Nat Protoc* 4, 767–782.
12. Han, Q., Bagheri, N., Bradshaw, E. M., Hafler, D. A., Lauffenburger, D. A., Love, J. C., (2012). Polyfunctional responses by human T cells result from sequential release of cytokines. *Proc. Natl. Acad. Sci. U. S. A.* 109.5:1607-1612.

13. Beiyuan, F., Li, X., Chen, D., Peng, H., Wang, J., and Chen, J. (2016). Development of Microfluidic Systems Enabling High-Throughput Single-Cell Protein Characterization.. *Sensors* 16.2 :232.
14. Daaboul, G.G., et al. (2010) High-Throughput Detection and Sizing of Individual Low-Index Nanoparticles and Viruses for Pathogen Identification. *Nano Lett.* 21(7): p. 21.
15. Avci, O., Ünlü, N. L., Özkumur, A. Y., and Ünlü, M. S., (2015). Interferometric Reflectance Imaging Sensor (IRIS)—A Platform Technology for Multiplexed Diagnostics and Digital Detection” *Sensors*, 15, 17649-17665.
16. Yurt, A., Daaboul, G. G., Connor, J. H., Goldberg, B. B., and Ünlü, M. S., (2012). Single Nanoparticle Detectors for Biological Applications..*Nanoscale* 4.3 :715-26.
17. Ahn, S., Freedman, D. S., Massari, P., Cabodi, M., and Ünlü, M. S., (2013). A Mass-Tagging Approach for Enhanced Sensitivity of Dynamic Cytokine Detection Using a Label-Free Biosensor. *Langmuir* 29. 17: 5369-5376.
18. Siddha, S. P. (2013). Fabrication of PN-Junction Diode by IC Fabrication process. *International Journal of Innovative Research in Science, Engineering and Technology*, 5567-5573.
19. Microchem. (n.d.). SU-8 3000 Permanent Epoxy Negative Photoresist. Westborough, MA 01581 USA: MicroChem Corp.